Natural loss of function of ephrin-B3 shapes spinal flight circuitry in birds

Baruch Haimson[1], Oren Meir[1], Reut Sudakevitz-Merzbach[1], Gerard Elberg[1], Samantha Friedrich[3], Peter V. Lovell[3], Sónia Paixão[2], Rüdiger Klein[2], Claudio V. Mello[3*] and Avihu Klar[1*]

1 - Department of Medical Neurobiology, IMRIC, Hebrew University-Hadassah Medical School, Jerusalem, 91120, Israel

2 - Department 'Molecules – Signals – Development, Max Planck Institute of Neurobiology, Am Klopferspitz 18, 82152 Martinsried, Germany

3- Department of Behavioral Neuroscience, Oregon Health and Science University, Portland, Oregon, USA.

* - Corresponding authors

Avihu Klar
Department of medical Neurobiology
Hadassah Medical School
The Hebrew University, Jerusalem
91120
Israel
avihu.klar@mail.huji.ac.il

Claudio V. Mello
Department of Behavioral Neuroscience
Oregon Health and Science University
Portland, Oregon
USA
melloc@ohsu.edu

Abstract

Flight in birds evolved through patterning of the wings from forelimbs and transition from alternating gait to synchronous flapping. In mammals, the spinal midline guidance molecule ephrin-B3 instructs the wiring that enables limb alternation, and its deletion leads to synchronous hopping gait. Here we show that the ephrin-B3 protein in birds lacks several motifs present in other vertebrates, diminishing its affinity for the EphA4 receptor. The avian *ephrin-B3* gene lacks an enhancer that drives midline expression, and is missing in galliforms. The morphology and wiring at brachial levels of the chicken embryonic spinal cord resemble those of *ephrin-B3* null mice. Importantly, dorsal midline decussation, evident in the mutant mouse, is apparent at the chick brachial level, and is prevented by expression of exogenous *ephrin-B3* at the roof plate. Our findings support a role for loss of ephrin-B3 function in shaping the avian brachial spinal cord circuitry and facilitating synchronous wing flapping.

Teaser:

Walking vs flying: Deciphering the organization and evolution of the neuronal network that controls wing flapping in birds.

Introduction

A critical aspect of locomotion is left-right coordination. Limb alternation is the predominant gait mode in some amphibians (salamanders), reptiles and terrestrial mammals, while synchronous movements are manifested in the legs of other amphibians (frogs) and some marsupials, and in the wings of bats and birds. Based on classical electrophysiological studies in cats and rodents, and genetic manipulations of cell fate and axonal trajectories in mice, a modified "half-center oscillator" model has been proposed that explains limb alternations in mammals (*1*). The core elements are mutually inhibitory neuronal centers on each side of the spinal cord that produce oscillatory excitatory output. This output is simultaneously transmitted to interneurons that innervate motoneurons, termed pre-motoneurons (pre-MNs). These include ipsilateral excitatory pre-MNs that activate motor activity on one side, and commissural inhibitory pre-MNs that inhibit motor output on the other side (Fig. 1A) (*2*).

The axon guidance molecule ephrin-B3 and its cognate receptor EphA4 are key regulators of alternating gait. In this family, ligand binding to the receptor typically results in axonal repulsion (forward signaling), but ephrin receptors can also act as ligands for ephrins (reverse signaling), prompting repulsion or adhesion (*3*). In wt mice, ephrin-B3 serves as a midline repulsive cue, preventing EphA4-expressing axons of excitatory pre-MNs from aberrantly crossing the ventral and dorsal midlines (Fig. 1A) (*4*). Transition from left-right alternation to synchrony occurs in mice mutated in the genes encoding ephrin-B3, EphA4*,* or the downstream signaling molecule α2-chimaerin. These mice, collectively referred to as *hopB3* mutants in this article, show ectopic commissural projections of otherwise ipsilaterally-projecting excitatory pre-MNs through the ventral and dorsal midlines (Fig. 1B) and walk with synchronous movements of the hind- and forelimbs, producing a hopping gait (*5-8*). Furthermore, impairment of the neuroepithelial organization of the roof plate (RP), which leads to partial absence of ephrin-B3 expression, results in rabbit-like hopping (*9, 10*).

Birds have evolved from dinosaurs that use alternating gait (*11*). Their adaptation for flight includes substantial structural specializations of the forelimb and of the spinal cord circuits that enable synchronous limb movements. Classical transplantation experiments in chick (our use of the term chick here refers to embryonic chicken) support a role for neuronal networks at the lumbar and brachial spinal levels in the control of the locomotion pattern of the hind- and forelimbs, respectively. In chicks where brachial segments are surgically replaced by lumbosacral segments, the movement of the wings become alternation, whereas coordinated flapping

movements are not observed (*12*). In the complementary experiment, transplantation of brachial segments to the lumbar cord result in synchronous, hopping-like leg movements (*13*). These findings support the hypothesis that local circuits in the lumbar and brachial spinal cord instruct level-specific alternate or synchronous movements, respectively.

Flight requires spinal circuits that enable the bilateral coordination of forelimb movements. It thus seems reasonable to hypothesize that the emergence of synchronous wing flapping in birds involved a transition from ipsilateral excitatory/contralateral inhibitory inputs to a pattern of bilateral co-excitatory input to wing motoneurons. Such a transition likely required changes in the pre-motor spinal wiring. Notably, mutations in the midline guidance molecules Netrin1 or ephrin-B3 in mice lead, respectively, to a reduction in cross inhibition and an increase in cross excitation (*5, 14, 15*). Netrins were initially described in chick, and have well characterized activity and roles in commissural axonal guidance (*16, 17*). However, little is known about ephrin-B3 in chick, and more generally in birds.

To explore a possible role of ephrin-B3 in locomotion patterns in birds, we have conducted a set of genomic, molecular and neuroanatomical studies, using both chick and zebra finch as experimental organisms. We found an ephrin-B3 gene ortholog (EFNB3) in several bird species and lineages, however their open reading frames (ORFs) were considerably shorter, and some domains critical for forward or reverse signaling were absent or heavily modified compared to non-avian tetrapods. We also observed marked loss of dorsal midline ephrin-B3 expression in the brachial spinal cord of zebra finch, likely due to an avian loss of a critical enhancer element. An EFNB3 ortholog could not be found in chicken and related species, suggesting a gene loss in galliforms. Spinal cord interneurons in chick showed extensive dorsal midline crossing at brachial levels, similar to ephrin-B3 null mice. In contrast, we observed little dorsal crossing at lumbar levels due to the presence of the glycogen body, which serves as a physical barrier to neurite crossing. The crossing at brachial levels was largely prevented by dorsal midline expression of mouse ephrin-B3. These findings are consistent with a role of ephrin-related mechanisms in spinal wiring patterns that may subserve limb alternation. They also support the notion that diminished barriers to dorsal midline crossing may have favored synchronous limb movements and facilitated the origin and/or maintenance of coordinated flight in birds.

Results

EFNB3 gene in birds

We have conducted an extensive and thorough analysis of the genomic region containing EFNB3 and syntenic genes in birds and non-avian outgroups. Our approach required extensive curation of gene predictions in annotated databases, permissive BLAST searches of genomes, WGS databases and p-reads (from Pacbio assemblies) using avian EFNB3 and syntenic gene queries, and RefSeq alignment searches of unplaced genomic scaffolds and reads (details in Methods). We found EFNB3 in a broad range of bird species and orders (see Methods for details on species names), including several songbirds, some eagles, an owl, a few cormorants, as well as the seriema, a hummingbird, the ruff, a crane, a stork, and some anseriforms (a duck and a goose). WRAP53 was immediately upstream of EFNB3 in all birds where synteny could be examined and in all non-avian organisms studied, including mammals, non-avian sauropsids and amphibians (major groups shown in Fig. 1C, synteny details for representative species shown in Fig. 1D), providing strong support for EFNB3 orthology. A gene prediction was present in only few species, whereas in several others EFNB3 was partial, possibly due to incomplete sequences in Illumina assemblies.

Notably, we could not identify EFNB3 in any galliforms (Fig. 1D, red square), even in species with high quality Pacbio assemblies and no local gaps. In chicken, the genes immediately syntenic to EFNB3 in other birds were either on chromosome 31 (KDM6B) or on an unplaced scaffold (WRAP53 and CHD3), with no trace of EFNB3 (Fig. 1D, chicken). This indicates that the syntenic genes are not adjacent in this species, but we cannot distinguish whether this resulted from an inter- or intra-chromosomal rearrangement compared to other birds. EFNB3 was also absent in the chicken WGS and Pacbio p-reads, and in numerous RNAseq databases. In a quail, a WRAP53 prediction and an unannotated KDM6B (found by BLAST) were found on the same incomplete scaffold. Several Pacbio p-reads from the current assembly (*18*) bridged the local gaps but revealed no trace of EFNB3 (Fig. 1D, Japanese quail). EFNB3 was also not detected in the assemblies or WGS of other galliforms (turkey, pheasant, guinea fowl), even though the syntenic genes were sometimes present in unplaced scaffolds (not shown). A scaffold in the unannotated genome of a grouse contained traces of WRAP53 and KDM6B but no evidence of EFNB3 sequences (Fig. 1D, Gunnison sage grouse). We also could not find EFNB3 in ratites, but the data were too sparse to conclusively prove or disprove an EFNB3 loss in this basal group.

Importantly, in most birds where EFNB3 synteny could be verified KDM6B was immediately downstream, whereas in non-avian sauropsids and mammals DNAH2 was interposed between

EFNB3 and KDM6B (Fig. 1D, blue). Given there were no gaps in several avian assemblies between EFNB3 and KDM6B, this observation supports an avian-specific loss of DNAH2, as previously indicated (*19*). As we show later, this finding has important implications for EFNB3 expression regulation. The exception among birds was the kakapo, where the receptor gene EphB4 was downstream of EFNB3, the only such case we are aware of. In sum, the EFNB3 gene is clearly present in a broad range of Neoaves, as well as in Anseriformes, but seems absent in Galliformes as a group (Fig. 1C,D). We suggest this is possibly due to a loss that occurred after their split from Anseriformes, estimated to have occurred between 55 to 72.5 million years ago (*20-22*), but prior to their later diversification.

EFNB3 gene and protein structure in songbirds

Songbirds were the avian group with the most complete information on EFNB3. In zebra finches, EFNB3 is largely conserved compared to non-avian tetrapods, consisting of 5 exons and a large 3'-UTR (*23*) (Fig. S1A). However, the percent identity of the predicted ephrin-B3 proteins in songbirds compared to human is low (48.9%-50.6%; Fig. S2), and their sizes are shorter compared to the amphibian, reptilian and mammalian proteins (247-267 vs 332-340 amino acid residues; Fig. S2). Functional domains in the extracellular and intracellular parts of the ephrin-B3 protein are missing in songbirds. In the intracellular domain, while the PDZ motif is intact, the entire SH2/3 binding motif, which is required for reverse signaling (*24, 25*), as well as the tyrosine residues that are phosphorylated upon activation of the reverse signaling in other organisms, are missing (Fig. 1E; Fig. S2), suggesting that reverse signaling is impaired. Birds also lack an extracellular heparin binding motif within the region juxtaposed to the transmembrane (TM) domain (*26, 27*), and several residues in the tetramerization interface within the receptor binding domain (RBD), required for normal signaling through the formation of receptor-ligand (Eph–ephrin) complexes (*28*) (Fig. 1E; Fig. S2). The region in the dimerization interface where an L to P (L111P) substitution leads to a hopping mouse phenotype (*29*) is conserved in birds and shows other substitutions (DLDL_108-111_QRDV) compared to mammals (Fig. S2). Unlike ephrin-B3, the predicted avian ephrin-B1 and ephrin-B2 proteins are highly similar to the mammalian proteins in terms of size, sequence and sub-domain partitioning. The mouse ephrin-B1 is 77.4% and 78% identical to the chicken and zebra finch proteins, respectively, and the mouse ephrin-B2 is 87.4% and 88.3% identical to the chicken and zebra finch proteins, respectively.

To test whether these structural differences affect cell trafficking of the avian ephrin-B3, we expressed an amino-myc tagged isoform of the mouse and zebra finch genes in COS-7 cells. Surface staining revealed that both proteins are presented on the cell membrane (Fig. 2A). Next, we used an assay where a chimeric protein composed of the extracellular domain of chicken EphA4 fused to placental alkaline phosphatase is tested for binding to different EFNB3 orthologs expressed in transiently transfected COS-7 cells, noting that chicken and the zebra finch EphA4 proteins share 98.4% identity (Fig. S3). We found that chicken EphA4 binds mouse ephrin-B3, but not zebra finch ephrin-B3 (Fig. 2B,C). Hence, the alterations in the sequence and structure of the extracellular domain of ephrin-B3 in songbirds have impaired its binding to the EphA4 receptor.

Expression of ephrin-B3 in zebra finch

The presence of EFNB3 gene in songbirds prompted us to examine its expression pattern in the zebra finch spinal cord. *In situ* hybridization with antisense riboprobes revealed ephrin-B3 mRNA expression in both the floor plate (FP) and roof plate (RP) of the brachial spinal cord in P0 zebra finches, with apparent lower expression in the RP (Fig. 2D). Quantification confirmed that ephrin-B3 expression is higher in the FP and declines along the RP in the ventral-to-dorsal direction (Fig. 2D'). This contrasted with mouse at a comparable developmental stage, where expression is similarly high in both the FP and RP (Fig. 2E), with no dorsal decline (Fig. 2E').

We reasoned that the modified ephrin-B3 expression seen in zebra finch compared to mouse might relate to changes in regulatory elements. Using UCSC's genome browser, we searched for enhancer hallmarks in mouse EFNB3 and its flanking genes. We also examined the existing mouse Hi-C datasets using an online tool (http://3dgenome.fsm.northwestern.edu/view.php; details in Methods). We found that mouse DNAH2, located immediately downstream of EFNB3 (Fig. 1D, blue), contains several features consistent with presence of an enhancer element in its 1st intron: binding of modified histones that are associated with enhancer elements, DNAaseI hypersensitivity, genomic conservation and the fact that the putative enhancer and the EFNB3 gene reside within the same topologically associating domain (TAD) (*30*) (Fig. S4). Because the DNAH2 gene is not present in birds (Fig. 1D blue; (*19*)), birds may lack an important EFNB3 enhancer element. To test whether this DNAH2-embedded region in mouse would be sufficient to confer midline RP expression in the spinal cord of a bird species, a reporter gene cloned downstream of the putative enhancer element was electroporated into the chick spinal cord at E3. Expression of the reporter in both the FP and RP

was evident at E9 and E15 (Fig. 2F,G), similar to mouse where endogenous ephrin-B3 midline expression occurs during embryogenesis and early post gestation (*5, 31*) (E15 chick is equivalent to mouse P2), and contrasting with the more ubiquitous expression of the co-electroporated GFP under a ubiquitous promoter (Fig. 2F,G, insets). Notably, *DNAH2* is missing in all bird species examined to date but it is present in reptiles (Fig. 1D; (*19*)), suggesting the loss of the EFNB3 regulatory element is specific to the avian lineage.

Expression of ephrin-B family ligands and EphA4 in chick spinal cord

We next used *in situ* hybridization to examine expression of ephrin-B1 and -B2 at the chick brachial cord, as both can mediate axonal repulsion through the EphA4 receptor and could thus potentially compensate for an EFNB3 loss. Both ephrin-B1 and B2 were expressed in the FP and RP at E10 (Fig. 3A,C). At E16, when the spinal circuitry elicits simultaneous wing flapping (*32*), ephrin-B1 expression persisted in the FP but dorsally it became restricted to the ventral aspect of the RP (Fig. 3B), whereas ephrin-B2 expression was detected only at the ventral tip of the RP (Fig. 3D). Expression of ephrin-B genes in chick spinal cord is thus largely restricted to the FP, low in ventral RP, and absent in the dorsal RP.

Next, we studied the expression of the receptor EphA4. In mouse, interneurons that express EphA4 are excluded from the dorsal midline, but many of these cells invade the dorsal midline in *EphA4* and *ephrin-B3* null mutants (*33*). In the chick, expression is detected throughout the spinal cord gray matter at E10, with high levels in scattered interneurons, in the lateral subdivision of the lateral motor column (LMC_l), and in the medial motor column (MMC), but absent in the dorsal midline (Fig. 3E). At E16, EphA4 shows high expression in discrete cells distributed all over the gray matter, including adjacent to and within the dorsal midline (Fig. 3F, white arrow in inset).

When we assigned x-y coordinates to EphA4-expressing cells, we observed their midline invasion at E16 compared to E10 (Fig. 3E',F',G). Thus, the presence of EphA4-expressing neurons in the dorsal midline correlates with the temporal reduction of ephrin-B1-2 levels. Taken together with the lack of ephrin-B3, we conclude that a molecular barrier that prevents midline crossing is missing in the chick dorsal spinal cord. This contrasts markedly with mouse, where midline expression of ephrin-B3 persists at high levels both ventrally and dorsally at post gestation stages (*5*).

Extended roof plate of the chick brachial cord

To further investigate how the natural loss of EFNB3 might have affected the organization of the avian spinal cord, we examined several parameters that differ significantly between wt and *hopB3* mutants, namely the size and axonal decussation at the RP, and the somata distribution and neurotransmitter phenotype of commissural pre-MNs (Figs. 4-6).

In wt mice, the length of the FP was relatively constant along the longitudinal axis, but the RP was substantially shorter at limb levels, resulting in low RP:FP ratios at those levels (Fig. S5). Thus, the RP:FP ratio can serve as a reasonable proxy for the size of the RP. The length of the RP at limb levels was markedly enlarged in EphA4 knockout mice (Fig. 4B,D) in comparison to control mice (Fig. 4A,C), with a significantly higher RP:FP ratio in the homozygous mutant (1.68±0.22, mean of RP:FP ratios ± SD) than in control mice (0.34±0.13). In birds, an elongated RP was evident at brachial levels in E15 chick (Fig. 4E) and P8 zebra finch (Fig. 4G), with RP:FP ratios of 2.18±0.2 and 1.53±0.08, respectively, thus comparable to EphA4 knockout mice (Fig. 4H). Hence, the morphology of the avian brachial RP is similar to that of *hopB3* mutants. At the lumbar sciatic level, the dorsal midline in birds is occupied by an ovoid gelatinous mass - the glycogen body (GB; Fig. 4F), an avian specific organ. Anatomical and histological studies demonstrate the presence of the GB in various bird species belonging to different clades (*34, 35*). These features differ from those in alternating limbed reptiles (lizard, turtle) where the RP is short, as in wt mice (*36, 37*), and no GB has been described.

Patterns of axonal midline crossing in the chick spinal cord

Axon fibers that cross the RP in rodents originate mostly from sensory neurons and inhibitory interneurons (*38, 39*). To further study the extent of dorsal midline crossing in the chick embryonic spinal cord, we examined immunoreactivity for neurofilament (3A10) and for sensory axons (TAG1) at E15 and E17. We observed neurofilament-positive axons crossing the brachial FP in a tight bundle (Fig. 5A, yellow arrows in insets), whereas those crossing the dorsal midline were less fasciculated and sparsely distributed along the dorsal RP (Fig. 5A, white arrows in insets). Quantification showed that 44.8±23% of midline crossing axons at the brachial level were in the RP (Fig. 5G, brachial). TAG1-expressing sensory axons did not appear to cross the midline at this level (Fig. 5B). To further interrogate midline axonal crossing, a membrane-tethered GFP was electroporated at E3 into one side of the spinal cord. At E15, GFP-labeled axons crossing the ventral and dorsal midline were evident (Fig. 5C, yellow and white arrows in insets). Interestingly,

a few labeled cells were apparent on the contralateral side dorsally, suggesting that some cells may migrate through the RP at the brachial level (Fig. 5C, white arrowheads in insets).

At the lumbar sciatic level, axonal decussation was apparent only through the FP (Fig. 5D-E), with no axons crossing the GB. At the lumbar crural level, which is devoid of GB, dorsal midline crossing was apparent, with 31±12% of crossing fibers occurring through the RP (Fig. 5F,G, crural). Notably, the sciatic nerve innervates muscles of the shank and foot, while nerves originating from the crural plexus innervate the thigh muscles (*40, 41*). Importantly, in the swing phase of birds, the ankle flexion leads to the elevation of the feet, while the knee is relatively stable. Hence, the sciatic nerve mediates the flexion and extension of the ankle and foot joints during stepping. Significant dorsal midline decussation was also apparent at the cervical, brachial and thoracic levels (Fig. 5G), as well as sacral levels (not shown), suggesting that the GB serves as a physical barrier for axonal decussation at the sciatic plexus level, thus allowing hindlimb alternation. In contrast, dorsal midline crossing at brachial levels correlates with synchronous wing (forelimb) movements, similar to that seen in *hopB3* mice.

Connectivity of pre-MNs in the chick spinal cord

The synchronous gait of *hopB3* mice results from ectopic midline crossing of excitatory pre-MN through the FP and RP (Fig. 1B) (*5, 42*). To analyze the patterns of connectivity of pre-MNs at the lumbar and brachial levels of the chick, we injected the trans-synaptic PRV virus (*43, 44*) into the leg, the distal wing musculature, and the main flight muscle, the pectoralis major. We observed substantial differences in the densities and laminar distributions of commissural pre-MNs (cpre-MNs) at lumbar versus brachial levels (Fig. 6A-C, right side). cpre-MNs accounted for 7.81% of labeled cells at the sciatic level, and for 25.3% and 34.8% of brachial level cells labeled from the distal wing and the pectoral muscle, respectively.

The distribution of ipsilateral pre-MNs (ipre-MNs) was similar at lumbar and brachial levels, occupying the medial spinal cord (Fig. 6A-C, left side; Fig. S6). In contrast, the distribution of cpre-MNs was markedly different across levels. At lumbar levels (both sciatic and crural) we observed cpre-MNs ventro-medially, with most cells ventral to the central canal (Fig. 6A, right side; Fig. S6). At the brachial level, cpre-MNs of the distal wing musculature and the pectoral muscle were distributed ventrally and dorsally to the central canal (Fig. 6B-C, right side). Likewise, decussation of pre-MNs differed markedly between lumbar and brachial levels, with axons crossing only the FP at the lumbar level (Fig. 6A'), but both the RP and the FP at the brachial level (Fig. 6B'-C').

Synchronous gait in mice *hopB3* mutants is also associated with pre-MNs that innervate motoneurons bilaterally (*42*). To directly test whether the chick brachial cord contains such cells, we injected PRV-GFP and PRV-cherry into the left and right pectoral muscles, respectively (Fig. 6D, left). 10.9% of pectoral cpre-MNs were double-labelled, most located above the central canal and adjacent to the dorsal midline (Fig. 6D), with neurite processes oriented toward the dorsal midline (Fig. 6D'). Hence, like in *hopB3* mice, a subpopulation of the brachial pre-MNs innervate motoneurons bilaterally (*42*).

To examine the neurotransmitter phenotype of spinal pre-MNs, we processed sections from hindlimb and wing PRV-injected embryos for *in situ* hybridization with a marker for excitatory neurons (vGlut2). At the lumbar level, 46.5% of the ipre-MNs and 38.6% of the cpre-MNs were excitatory. At the brachial level, 35% of the ipre-MNs and 38% of the ventral cpre-MNs were excitatory. Of the brachial-specific cpre-MNs that reside dorsal the central canal, 47% were excitatory (Table S1, Fig. S7). The chick brachial-specific pre-MNs are thus comparable to the ectopic cpre-MNs in *hopB3* mutants in location, wiring and excitatory phenotype (*10, 42*).

Exogenous ephrin-B3 expression in the chick RP prevents midline axonal crossing

Our observations so far suggest that dorsal midline crossing and the wiring pattern of brachial pre-MNs in chick spinal cord might be linked to a lack of ephrin-B3 expression due to the genomic loss. To test this hypothesis, we examined whether expression of mouse ephrin-B3 in the chick would affect RP neurite crossing. Mouse ephrin-B3 or GFP, cloned into a Cre-dependent expression vector under the RP-specific Wnt1 enhancer element (*45*), were co-electroporated into the E3 chick spinal cord (Fig. 7A), and the extent of RP neurite crossing analyzed at E15. To exclude possible effects of exogenous ephrin-B3 in reverse signaling, we also used an ephrin-B3 isoform that lacks the intracellular domain (ephrin-B3-ΔC). Ephrin-B3 expression was confined to the RP (Fig. 7B), and the number of midline crossing neurites was significantly lower for ephrin-B3 (7.1 ± 3.1) or ephrin-B3-ΔC (7.1 ± 2.6) than for GFP (16.5 ± 4.6) (Fig. 7C-E). Hence, as in mammals, midline ephrin-B3 expression through forward signaling (*5, 8*) is sufficient to prevent midline crossing.

Next, after targeting ephrin-B3 expression to the RP at E3, PRV was injected into the wing musculature at E14 (Fig. 8A), and the numbers and distribution of cpre-MNs examined at E15.5. In controls, both ipre-MNs and cpre-MNs were seen, the latter both dorsal and ventral to the central canal (Fig. 8B), and their neurites crossed at both the FP and RP (Fig. 8B'). In ephrin-B3-expressing

embryos, fewer cpre-MNs were seen dorsal to the central canal (Fig. 8C,C',C'',D,E), and most neurites were observed to cross the FP (Fig. 8C,C',C'', right insets). Short cell extensions, possibly dendrites originating from ipre-MNs, did cross the RP (Fig. 8C, C', right insets). We note that *in ovo* electroporation results in mosaics where only a portion of the cells express the transgene. Our efficiencies, assessed as sections with midline expression of ephrin-B3, varied from 5% to 64% (Fig. 8D), thus axons circumvent ephrin-B3 and cross the midline close to non-EFNB3 expressing RP cells (Supp. Movie S1). The ectopic expression of ephrin-B3 did not affect the dorsoventral extent of the RP (Fig. 7C,D; Fig. 8B,C). The mosaic non-continuous expression of the exogenous ephrin-B3, attained via *in ovo* electroporation, may explain the lack of an effect on the size of the RP, in the manipulated chicks.

Next, we analyzed the spatial distribution of cpre-MNs in five embryos with variable efficiencies of wnt1::ephrin-B3 expression (Fig. 8D). A dorsal to ventral shift in the location of cpre-MNs was apparent when comparing the embryos with lower vs higher exogenous ephrin-B3 expression in the RP (1-3 vs 4-5 in Fig. 8D), suggesting a reduction in the size of the brachial-specific dorsal population of cpre-MNs. To further quantify this observation, we subdivided cpre-MNs into ventral and dorsal groups, based on location relative to the central canal, and examined their numbers compared to ipre-MNs. The distribution of pre-MNs in three GFP-expressing embryos served as control. The percent of dorsal cpre-MNs from the total number of pre-MNs was calculated and correlated with the efficiency of midline expression of ephrin-B3, using linear regression (Fig. 8E, Table S2); the average number of pre-MNs in the three GFP-expressing embryos was included as having null midline ephrin-B3 expression efficiency. The Pearson correlation coefficient between efficiencies of ephrin-B3 expression and the percent of dorsal cpre-MN was - 0.95 ($p=0.0035$). Thus, the dorsal cpre-MNs population is reduced in proportion to higher ephrin-B3 expression at the RP.

We also calculated the ratios between pre-MNs populating the different zones (ventral cpre-MNs, dorsal cpre-MNs and ipsi pre-MNs) and correlated these ratios with the efficiencies of midline ephrin-B3 expression (Fig. S8). The ratio of ventral cpre-MNs to ipre-MNs was similar in controls and all experimental embryos (Fig. S8A), thus ephrin-B3 RP expression did not affect this population. The ratio of dorsal cpre-MNs to ipre-MNs was reduced in proportion to higher ephrin-B3 expression (Fig. S8B), as was their ratio to ventral cpre-MNs (Fig. S8C). The ratio of all cpre-MNs to the ipre-MNs was also negatively correlated with increasing ephrin-B3 expression (Fig. S8D). We

conclude that robust ephrin-B3 RP expression results in fewer dorsal cpre-MNs that cross through the RP, while ventral cpre-MNs that cross through the FP are not affected.

Discussion

During vertebrate evolution, most terrestrial species adopted alternating limb motion as an effective gait strategy, while adaptation to powered flight in birds emerged via morphological changes that patterned wings from forelimbs, and required transition from alternate gait to synchronous flapping. Our genomic analysis indicates that the gene encoding the midline axonal repellent ephrin-B3 is missing in chicken and other galliforms. In songbirds, the EFNB3 gene encodes an ephrin-B3 protein that does not bind to the EphA4 receptor, and whose expression in the spinal cord is reduced along the roof plate, probably due to the loss of a downstream enhancer. Morphological and circuit analyses revealed that the chick spinal cord shares similarities with wt mice at the lumbar level (Fig. 9A,C), and with *hopB3* mutant mice at the brachial level (Fig. 9B,D). Importantly, dorsal midline expression of exogenous (rodent) ephrin-B3 in the chick brachial spinal cord prevents crossing of cpre-MN axons (Fig. 9E). Altogether, our findings support the notion that a reduction in ephrin-B3 expression and/or function plays an important role in shaping the wing level circuitry in the avian spinal cord.

Loss of ephrin-B3 function in birds

Changes in gene copy number, enhancers, and protein sequence, arguably some of the foremost molecular events in evolution, are thought to have influenced locomotion patterns in vertebrates. For example, a point mutation that leads to a premature stop codon in *DMRT3* enabled Icelandic horses to develop their characteristic Tölt ambling gait (*46*). A modification and subsequent loss of a regulatory element of *GDF6* during the transition to bipedalism in humans is thought to have played a role in foot digit shortening (*47*). Limb loss in snakes has been shown to be a result of mutations in a limb-specific enhancer of Sonic hedgehog (*48*). Loss of function for ephrin-B3 leads to midline crossing in the spinal cord of rodents, resulting in a remarkable hopping gait (*5, 6*). Our findings now indicate that the ephrin-B3 gene has undergone significant modifications in birds compared to non-avian groups, likely impacting flight control circuits in the avian spinal cord. Absence of *DNAH2* is seen in all birds where this genomic region could be assessed, suggesting that the loss of a putative ephrin-B3 enhancer was an early event in avian evolution, or possibly even in dinosaurs. It seems reasonable to hypothesize that the enhancer loss preceded the loss/degradation of functional domains, but at present it is hard to conclusively answer that question given the lack of data on EFNB3 gene structure and synteny in the most basal avian clade, Palaeognathae. The enhancer that we characterized is probably also not the only EFNB3

expression regulator, since zebra finches show endogenous EFNB3 expression in the FP. Targeted deletion of the *DNAH2*-embedded enhancer from the mouse genome may further reveal its contribution to the pattern and level of EFNB3 expression. The apparent loss of EFNB3 in chicken and other galliforms was likely a more recent event specific to that basal clade, since EFNB3 is present in Anseriformes and in several Neoaves, including the more recently evolved Passeriformes. It is hard to estimate the timing of mutations in the coding region, since high quality sequence is limited to a few species. Nonetheless, similar protein changes compared to mammals and non-avian sauropsids are present in eagles and in songbirds (Fig. S2), avian groups whose split from their sister taxa is estimated to have occurred ~63-64 and ~55-61 million years ago, respectively (*20-22*). High-quality sequences of this region in other avian clades will be critical for better understanding the timing and extent of avian EFNB3 changes.

In zebra finch, besides a predicted lack of reverse signaling due to loss of specific domains, we provide clear evidence that forward signaling through the EphA4 receptor is impaired. The lack of binding to avian EphA4, for example, is likely related to substitutions in residues 108-111 (in the mouse protein). This region is within the G β-strand which forms a loop with the H β-strand, and is part of the ligand-receptor dimerization interphase (*49*). Interestingly, in amphibians and non-avian sauropsids this region is also quite divergent compared to mammals (Fig. S2), even though other domains are more conserved than in birds. Future experiments utilizing chimeric protein constructs across these groups may reveal further insights into the evolution of ephrin-B3 and its possible role in controlling spinal cord wiring and pattern of locomotion across vertebrates. We also note that we currently do not know whether the lack of functional domain in the intracellular portion of avian ephrin-B3 causes impairments to other functions that depend on reverse signaling in ephrin-B3-expressing cells.

Phenotype of avian and *hopB3* mouse spinal cords

Our data show that the brachial spinal cord in chicken, which lacks an EFNB3 gene, shares similarities with mouse *hopB3* mutants in its morphology, and in the wiring and excitatory/inhibitory balance of cpre-MNs (Fig. 9B,D). The significance of the dorsal midline expansion, anatomically the most profound alteration in *hopB3* mutants, is unclear. While synchronous motoneuron activity is seen in the spinal cord of *hopB3* mutants using an *in vitro* fictive locomotion assay, severing of the dorsal midline does not restore left-right alternation (*4, 50*), arguing that bilateral coupling is facilitated by ventral midline crossing. However, *in vivo*

disruption of the roof plate integrity is sufficient to induce synchronous gait in mice (*9, 10*). It is conceivable that in *hopB3* mutants, proprioceptive signals from weight-load receptors, which are used only *in vivo*, inhibit the bilateral coupling mediated by the dorsally crossing axons. In support of this hypothesis, removal of EphA4 from a subpopulation of dorsal interneurons results in ectopic dorsal midline crossing. Furthermore, the over-ground gait of these mice is normal, while during air-walking and swimming their limbs move in synchrony (*42*). In birds, dorsal midline crossing might be sufficient to instruct the bilateral coupling of the wings motoneurons, since weight load without ground support during flight does not affect the wings.

The importance of excitatory neurons for synchronous gait in mouse *hopB3* mutants is shown by conditional targeting of EphA4 in vGlut2 neurons, which results in hopping gait (*4*). Furthermore, a rather small shift in the excitatory/inhibitory balance in cpre-MNs, from 21% excitatory and 46% inhibitory in wt to 26% and 35% in the EphA4 null mouse, is sufficient to induce synchronous gait (*4, 50*). We found that the brachial dorsal population of cpre-MNs in chick is moderately but significantly more enriched (–47%) with excitatory neurons than in wt mice. Furthermore, the difference between this population and the brachial ventral and lumbar cpre-MNs, both corresponding to ~38% of excitatory neurons (Fig. 6, Table S1), is similar to the difference between wt and *hopB3* mutant mouse. These observations support the notion that the brachial-specific population of cpre-MNs is sufficient to support synchronous activation of motoneurons involved in wing flapping.

Intriguingly, *t*he glycogen body (GB) (Fig. 8I) is a prominent but poorly understood dorsal lumbar gelatinous structure that arises from roof plate cells, is present across birds, and may have been present in dinosaurs (*34, 35, 51*). Our study has uncovered evidence that the GB serves as a major physical barrier to dorsal midline crossing at sciatic lumbar levels in the chick. We thus suggest that the GB is likely a major contributor to the alternating gait in birds, analogous to the molecular barriers to midline crossing in mice. Further comparative studies are needed to further elucidate the exact role of the GB across birds with predominantly hopping versus alternating gaits.

Alternative mechanisms and further comparative notes

Our findings do not exclude the possibility that other genetic mechanisms might play important roles in shaping avian spinal circuits underlying synchronous wing movement. For example, some molecular pathways involved in midline crossing at the FP have been described as

missing or altered in birds. DCC, a receptor for the axon guidance modulator Netrin-1, is missing in chicken and zebra finch, but is preserved in other avian groups like ducks (*52-54*). Robo3, a receptor for Slit ligands that are involved in axonal guidance and required for midline crossing, shows distinct features in birds compared to mammals. While avian Robo3 binds Slits, mammalian Robo3 specifically interacts with DCC (*55*). Presently, it is unclear whether these modifications contribute to species-specific spinal functions, or whether they preceded or followed the ephrin-B3 function loss described here. Other mechanisms that could contribute to modulation of flight-related circuitry also remain to be investigated, including changes in synaptic input, axonal trajectory or neurotransmitter identity of the interneuron populations involved in the alternation-to-synchronization transition.

Some vertebrate lineages other than birds have evolved synchronous limb movement, including flight in bats, hopping in post-morphogenesis anurans (frogs and toads) and macropods (kangaroos and wallaby). Protein alignment revealed high levels of conservation of bat and wallaby ephrin-B3 compared to mouse (Fig. S2). Thus, mechanisms unrelated to ephrin-B3 changes are more likely to instruct synchrony-mediating spinal circuitry in these mammals. In amphibians, ephrin-B3 conservation compared to mouse is higher for salamander, which walks via alternation, than for anurans (Fig. S2). Studies of ephrin-B3 expression and activity in amphibians are needed to test whether modulation of this signaling pathway has shaped the spinal circuitry for synchronous leg movements in anurans. Lastly, we note that due to technical limitations, it has not been possible to directly assess the role of this pathway in avian flight behavior. Approaches other than electroporation, such as germline transgenesis, will likely provide a more suitable experimental paradigm to test the physiological role of ephrin-B3 gain of function in birds like chicken or quail.

In summary, we provide evidence linking loss of ephrin-B3/ EphA4 signaling to the emergence of synchrony-mediating circuitry in the avian brachial spinal cord. While our findings do not exclude the importance of other molecular pathways, they suggest that modulation of ephrin-related mechanisms may have been an important contributor to the origin of flight in birds.

Materials and Methods

Genomics

The EFNB3 genomic region in birds has presented several difficulties for sequencing and assembling, likely due to very high GC content and density of poorly characterized repeat elements. The gene and its syntenic region are not present, or present only in partial form, in most Sanger- and Illumina-based avian assemblies, but are better represented in the more recent PacBio assemblies (*23, 56*). Furthermore, this region is likely part of a short avian micro-chromosome, which until the recent Swainson's thrush (*Catharus ustulatus*) genome had not been assembled and/or annotated in any species. Our current study of EFNB3 in birds has therefore required considerable search, annotation and curation efforts.

Briefly, we initially examined the annotated databases (NCBI's RefSeq, Ensembl) available for >50 avian species, searching for gene predictions annotated as EFNB3 or ephrin B3-like, and using reciprocal BLAT alignments and verification of conserved synteny of the predictions to confirm their orthology with humans and non-avian vertebrates (e.g. green anole - *Anolis carolinensis*, Chinese alligator - *Alligator sinensis*). We were able to identify EFNB3 and to verify its orthology in several songbird species (zebra finch – *Taeniopygia guttata*, Bengalese finch - *Lonchura striata domestica*, common starling - *Sturnus vulgaris*, Tibetan ground-tit - *Pseudopodoces humilis*, Small tree finch - *Camarhynchus parvulus*, Swainson's thrush - *Catharus ustulatus*), in the golden eagle (*Aquila chrysaetos*) and bald eagle (*Haliaeetus leucocephalus*), and in a parrot, the kakapo (*Strigops habroptilus*). Notably, in the Swainson's thrush EFNB3 and syntenic genes have been assigned to chr37, the first case any genes have been assigned to that avian micro-chromosome. We also note that two apparently identical zebra finch EFNB3 models (discontinued Gene IDs: 115492780 and 115492629) were present in an unplaced scaffold (NW_022045341.1) of an early PacBio assembly (bTaeGut1_v1.p; (*56*), but have been recently discontinued as this entire region is not present in the latest zebra finch Pacbio assemblies in NCBI (as of March 2021). We used the discontinued XM_030261704.1 transcript prediction in our study, noting that it is well supported by ESTs and transcriptome data (Fig. S1A,B). Ensembl has EFNB3 predictions for the zebra finch, kakapo, and the Eurasian sparrowhawk (*Accipiter nisus*), the latter in a short segment and right upstream of KDM6B. We also BLAST searched avian and non-avian RefSeq databases using as queries the genomic regions just downstream of avian gene predictions annotated as WRAP53 (or WD repeat containing antisense to TP53, a.k.a. telomerase Cajal body protein 1), or just upstream of avian gene predictions for KDM6B (or lysine specific demethylase

6B). This effort identified EFNB3 in the barn owl (*Tyto alba*) and in another songbird species, even though no EFNB3 predictions were present. We also BLAST searched all existing avian genomes (May 2020) as well as the respective WGS databases, using as queries the existing avian EFNB3 predictions, and manually examined all hits with scores >50, excluding cases that did not show top reciprocal alignments (typically other EFNB family members). This effort identified EFNB3 in the double-crested cormorant (*Phalacrocorax auritus*), and in a few other passerines and anseriforms with limited synteny information, as well as in several species with incomplete data for synteny verification (mallard - *Anas platyrhynchos*, swan goose - *Anser cygnoides*, several other passerines, other cormorants, the red-legged seriema - *Cariama cristata*, the ruff - *Calidris pugnax*, the grey crowned-crane - *Balearica regulorum*, and the Oriental stork - *Ciconia boyciana*). As an EFNB3 was not present in the current Anna's hummingbird (*Calypyte anna*) PacBio assembly (the only such case for a non-galliform avian PacBio assembly), we also BLAST searched the pre-assembled reads (p-reads) for this assembly, and obtained evidence for an ortholog with similar synteny as in other bird groups. We also conducted BLAST searches for EFNB3 in the current assemblies of chicken (*Gallus gallus*; Pacbio-based GRCg6a) and Japanese quail (*Coturnix japonica*; hybrid Coturnix japonica 2.1), as well as in the corresponding Pacbio p-reads and previous assemblies. Similar searches were also conducted in the Illumina-based assemblies and WGS databases of other galliforms, namely turkey (*Meleagris gallopavo*), golden pheasant (*Chrysolophus pictus*), helmeted guineafowl (*Numida meleagris*), and Gunnison sage grouse (*Centrocercus minimus*). These searches were extensive and permissive (>30 hit scores), followed by manual verification of detected hits. We also searched the BBSRC ChickEST Database and several brain transcriptome databases at E10, E17, P0 and 10 weeks old chick available in NCBI (ERR2576391, ERR2576392, ERR2576465, ERR2576464, ERR2576488, ERR2576584, ERR2576585, ERS2480079), but found no evidence of EFNB3.

The predicted ephrin-B3 proteins that were used for the proteins alignment (Fig. S2) were derived from the following: Human (*Homo sapiens*) - Accession: NM_001406.4; Mouse (*Mus musculus*) - NM_007911.5; Egyptian fruit bat (*Rousettus aegyptiacus*) – XM_016154770; Wallaby (*Macropus eugenii*) – from two EST clones FY22448 and FY578350; Chinese alligator – XM_02519434; Chinese softshell turtle (*Pelodiscus sinensis*) – XM-025188382; Iberian ribbed newt (*Pleurodeles waltl*) – Trinity_DN303912 (*57*); African clawed frog (*Xenopus Laevis*) – XM_018239717; Tibetan frog (*Nanorana parkeri*) XM_018574039); Zebra finch (*Taeniopygia guttata*) – Fig. S1, Small tree finch (*Camarhynchus parvulus*) - XM_030970743; Swainson's thrush

(*Catharus ustulatus*) – XM_033084252; Starling (Sturnus vulgaris) – XM_014893375; kakapo (Strigops habroptilus) – XM_030474552.

Animals

Fertilized White Leghorn chicken eggs (Gil-Guy Farm, Israel) were incubated in standard conditions at 38 °C. Zebra finch hatchlings were obtained from Anat Barnea (Department of Natural and Life Sciences, The Open University of Israel, Ra'anana 43710, Israel; School of Zoology, Tel-Aviv University). All experiments involved with animals were conducted in accordance with the designated Experiments in Animals Ethic Committee policies and under its approval. Experiments were performed on adult male and female mice. EphA4^{lox} mice (*58*) were crossed to PGK-Cre mice (*59*) to generate full knock-out of the EphA4 gene. Animals were kept and used in accordance with regulations from the government of Upper Bavaria.

DNA

For the binding assay in COS cells, the mouse ephrin-B3 was cloned into pSecTag-B plasmid (Termo Fisher Scientific, Waltham, USA). Six repeats of the myc epitope were cloned at the carboxyl end of ephrin-B3. For cell surface detection of the mouse ephrin-B3, the kappa chain signal sequence plus 3 repeats of the myc epitope were cloned upstream to amino acid 30 of the mouse gene. The sequence of the full-length zebra finch ephrin-B3 transcript was reconstructed from RNA-seq reads (Fig. S1B,C) using the Trinity platform (*60*). The sequence matched the exonic sequence of the EFNB3 transcript prediction (XM_030261704.1). For cloning the zebra finch ephrin-B3, an optimized sequence (available upon request) of residues 21-171 (Fig. S2), predicted to encode the extracellular domain, was synthesized (ITD, Coralville, USA) and cloned downstream to an Ig kappa chain signal sequence in the pSecTag-B plasmid. The transmembrane and intracellular portions of the zebra finch transcript were obtained by fully sequencing the EST DV945855 cDNA clone. The synthetic 5' portion of the gene plus the 3' DV945855-derived sequence were fused using a PCR-generated EcoRV site at the synthetic 5' part and an internal SmaI site in the 3' DV945855-derived sequence. For detection of the *in vitro* transcribed protein, 4 repeats of the myc epitope were inserted between the Ig kappa chain signal sequence and predicted residue 21 of zebra finch ephrin-B3. The EphA4-AP fused gene was generated by cloning amino acids 1-543 of the chick EphA4 (*61*) into the pSecTag-B plasmid. The SEAP gene was cloned downstream to EphA4.

Cell culture and transfection

COS-7 cells (ATCC) were cultured in DMEM media (Sigma, Saint Louis, USA) supplemented with 10% fetal bovine serum 100U/ml penicillin, 100 mg/ml streptomycin and 2 mM glutamine (Biological industries, Beit HaEmek, Israel). COS-7 cells were transiently transfected with appropriate cDNA using PEI (Polyethylenimine, linear, MW 25000; Polysciences, Inc).

AP-fusion protein binding experiments

To produce secreted EphA4-AP (alkaline phosphatase, placental) fusion protein, COS-7 cells were transiently transfected with appropriate cDNA. Post-transfection cells were supplemented with Opti-MEM (Gibco), and media collected after 48 hr. The media was concentrated through a 30K ultracell filter (Merck Millipore, Tullagreen, Ireland). The amount of the AP fusion protein was quantified by SDS-PAGE analysis and Coomassie staining. The amount of EphA4-AP was calibrated by comparison to known amounts of EphA4-Fc fusion protein (R&D, Indinapolis, USA). AP activity was measured using para-nitrophenylphosphate substrate (pNPP, Sigma).

Binding assays were carried in COS-7 cells, transiently transfected with the mouse or zebra finch ephrin-B3. Following over-night (O/N) incubation, cells were incubated with varying amount of EphA4-AP in binding buffer (Hanks buffer saline supplemented with 20 mM Hepes, PH 7.3, 0.05% BSA, 5 mM CaCl2, 1 mM MgCl2 and 10 µg/ml heparin sodium salt (Sigma) at room temperature (RT) for 70 min. For visualization of AP staining, cells were plated on glass coverslip coated with poly-lysine (0.005%, Sigma), and following AP-ligand binding as described above, cells were washed with-binding buffer, fixed in 4% paraformaldehyde (PFA) in PBS for 15 min at RT, and then washed with HBS solution (20 mM HEPES pH 7.3, 150 mM NaCl). Endogenous AP activity was inactivated by incubation at 65 °C for 100 min. For color reaction, cells were incubated with NBT/BCIP substrates (Roche, Basel, Switzerland) in AP buffer (100 mM Tris pH 9.5, 100 mM NaCl, 5 mM $MgCl_2$), O/N. After washing in HBS and fixation for 15 min in 4% PFA, and an additional washing in HBS, coverslips were mounted under mounting medium (Thermo Scientific, USA).

For colorimetric assays, following AP-ligand binding and washing, cells were incubated O/N at 4°C in lysis buffer (10 mM Tris, ph 8.0, with 1% Triton X100). The supernatant was subjected to heat inactivation for 15 min at 65°C. Lysates were transferred to 96-well high protein absorbance plate (Thermo Scientific, Nunc International USA) and the level of AP activity was determined following addition of equal volume of 2 mg/ml pNPP substrate in reaction buffer (200 mM Tris, pH

9.5, 10 mM MgCl2, 200 mM NaCl). Plates were incubated at RT for 30 min to 1 hr and optical density was determined at 405 nM using an ELISA plate reader.

Ephrin-B3 surface staining

COS-7 cells were transiently transfected with the mouse or zebra finch myc-EphrinB3 expression vectors. 24 hr post-transfection, cells were incubated with mouse anti-myc (9E10) antibody in phosphate buffered saline (PBS), washed with PBS, and subsequently incubated with Rhodamine Red X (RRX) labeled anti-mouse antibody and washed again. Cells were fixed in 4% paraformaldehyde/0.1 M phosphate buffer and mounted before imaging.

In-ovo electroporation

A DNA solution of 5 mg/mL was injected into the lumen of the neural tube at HH stage 17– 18 (E2.75-E3). Electroporation was performed using 3 × 50 ms pulses at 25–30 V, applied across the embryo using a 0.5 mm tungsten wire and a BTX electroporator (ECM 830). Following electroporation, 150–300 µL of antibiotic solution, containing 100 unit/mL penicillin in Hank's Balanced Salt Solution (Biological Industry, Beit-Haemek) was added on top of the embryos. Embryos were incubated for 3–19 days prior to further treatment or analysis. Roof plate-specific expression was achieved utilizing the Wnt1 or DNAH2 enhancers, coupled with a dorsal electrode positioning.

Immunohistochemistry and *in-situ* hybridization

Embryos were fixed overnight at 4°C in 4% paraformaldehyde/0.1 M phosphate buffer, washed twice with phosphate buffered saline (PBS), incubated in 30% sucrose/PBS for 24 h, and embedded in OCT (Scigen, Grandad, USA). Cryostat sections (20 µm) were collected on Superfrost Plus slides and kept at −20°C. For thicker sections, spinal cords were isolated from the fixed embryos and subsequently embedded in warm 5% agar (in PBS), and 100 µm sections (E12–E17) were cut with a Vibratome. Sections were collected in wells (free-floating technique) and processed for immunolabeling. The following primary antibodies were used: rabbit polyclonal anti-GFP 1:1000 (Molecular Probes, Eugene, Oregon, USA), mouse anti-GFP 1:100, goat anti-GFP 1:300 (Abcam, Cambridge, UK), rabbit anti-RFP 1:1000 (Acris, Hiddenhausen, Germany), goat anti-ChAT 1:300 (Cemicon, Temecula, CA, USA), mouse anti TAG1 4-5 (DSHB, University of Iowa), mouse anti-neurofilament 1:100 (3A10), mouse anti-myc 1:10 (9E10), rabbit anti-myc 1:100 (Abcam). The

following secondary antibodies were used: Alexa Fluor 488/647-AffiniPure Donkey anti-mouse, -rabbit and -goat (Jackson), and Rhodamin Red-X Donkey anti-mouse and -rabbit (Jackson). Images were taken under a microscope (Eclipse Ni; Nikon) with a digital camera (Zyla sCMOS; Andor) or a confocal microscope (FV1000; Olympus).

In situ hybridization was performed as described (Avraham et al., 2010). The following probes were employed: chicken ephrin-B1, ephrin-B2, EphA4 and Vglut2, zebra finch ephrin-B3 and mouse ephrin-B3. Probes were PCR-amplified from brain cDNAs of E6 chicken embryo, P4 zebra finch, and E15 mouse, respectively, using the following primers (Table 1). PCR products were verified by sequencing prior to use.

Table 1: List of primers that were used for generating the RNA probes

Name	Sequence
cEFNB1-F	GAAAAAGGACCAGGCAGATGC
cEFNB1-R-T7	AGCTAATACGACTCACTATAGTTCTCTGTAGTCCGTAAGGG
cEFNB2-F	GAGGGGTGTGCCAGACAAAA
cEFNB2-R-T7	AGCTAATACGACTCACTATAGCACTGTCTGCAGTCCTTAGAG
cEPHA4-F	ACAGGCCCAATGGAGTCATC
cEPHA4-T7	AGCTAATACGACTCACTATAGGCATCCAAGGAGCCATTCTC
mEFNB3-F2	CCAGAACAGGAAGTCGCACT
mEFNB3-T7	AGCTAATACGACTCACTATAGCAAGACAAATTGGGCCTGCC
vGlut2-F	GGAAGATGGGAAGCCCATGG
vGlut2-T7	GAAGTCGGCAATTTGTCCCC
zfEFNB3_3'-F-T3	GCAATTAACCCTCACTAAAGGCACGCCCACAAAGGGAAGGA
zfEFNB3_3'-R-T7	AGCTAATACGACTCACTATAGTCTAATCAGCAGCAGCCGCG
zfEFNB3_5'-F-T3	GCAATTAACCCTCACTAAAGGTTACGTGCTGTACCCGCAGAT
zfEFNB3_5'-R-T7	AGCTAATACGACTCACTATAGCTCGTCTGATTGGCTGAACCT

PRV injection

We used two isogenic recombinants of an attenuated PRV strain (PRV Bartha) that express enhanced GFP (PRV152) and monomeric red fluorescent protein (PRV614). The viruses were harvested from Vero cell cultures at titers 4 × 108, 7 × 108 and 1 × 109 plaque forming units (pfu/mL), respectively. Viral stocks were stored at −80°C. For pre-motoneuron infection, injections of 3 µL of PRV152 or PRV614 were made into the thigh or wing musculature of E13 or E14 chicken embryos, using Hamilton syringes (Hamilton; Reno, NV, USA) equipped with a 33-gauge needle. The embryos were incubated for 36–40 hr and sacrificed for analysis. For bilateral pre-motoneurons infection, PRV152 and PRV614 were each injected into the pectoralis musculature on opposite sides of the embryo midline.

Cell distribution and density plots construction

The codes for the cell distribution and density plots imaging and analysis were written in Matlab. The distribution plots were constructed by calculating the relative midline expression, after background subtraction and a subsequent length normalization between all analyzed sections. The density plots were generated based on cross section images transformed to a standard form. The background was subtracted, and the cells were filtered automatically based on their soma area or using a manual approach. Subsequently, the neurons were depicted by semi-transparent circles or their distribution was visualized by two-dimensional kernel density estimation, using the MATLAB function “kde2d”. Unless indicated otherwise, a contour plot was drawn for density values between 20% and 80% of the estimated density range, in six contour lines. An additional script was used for pre-motoneuron classification based on their neurotransmitter identity and laminar location.

A similar density visualization procedure was done for the EphA4 density plots (Fig. 3E’ and F’), but was preceded by signal binarization and then an averaging filter (5 cycles) was used to achieve a smoother density signal. The intensity of EphA4 signal as a function of distance from the midline was obtained by summation of the binary signal over the horizontal axis, followed by a rescaling step for each image. The difference at the midline between the intensity profiles of E10 and E16 data was evaluated by t-test.

References

1. T. G. Brown, On the nature of the fundamental activity of the nervous centres; together with an analysis of the conditioning of rhythmic activity in progression, and a theory of the evolution of function in the nervous system. *J Physiol* **48**, 18-46 (1914).
2. S. Grillner, T. M. Jessell, Measured motion: searching for simplicity in spinal locomotor networks. *Curr Opin Neurobiol* **19**, 572-586 (2009).
3. A. Kania, R. Klein, Mechanisms of ephrin-Eph signalling in development, physiology and disease. *Nat Rev Mol Cell Biol* **17**, 240-256 (2016).
4. L. Borgius *et al.*, Spinal glutamatergic neurons defined by EphA4 signaling are essential components of normal locomotor circuits. *J. Neuroscience* **34**, 3841-3853 (2014).
5. K. Kullander *et al.*, Role of EphA4 and EphrinB3 in local neuronal circuits that control walking. *Science* **299**, 1889-1892 (2003).
6. K. Kullander *et al.*, Ephrin-B3 is the midline barrier that prevents corticospinal tract axons from recrossing, allowing for unilateral motor control. *Genes Dev* **15**, 877-888 (2001).
7. H. Wegmeyer *et al.*, EphA4-dependent axon guidance is mediated by the RacGAP alpha2-chimaerin. *Neuron* **55**, 756-767 (2007).
8. N. Yokoyama *et al.*, Forward signaling mediated by ephrin-B3 prevents contralateral corticospinal axons from recrossing the spinal cord midline. *Neuron* **29**, 85-97 (2001).
9. K. Katayama, J. R. Leslie, R. A. Lang, Y. Zheng, Y. Yoshida, Left-right locomotor circuitry depends on RhoA-driven organization of the neuroepithelium in the developing spinal cord. *J Neurosci* **32**, 10396-10407 (2012).
10. S. Skarlatou *et al.*, Afadin Signaling at the Spinal Neuroepithelium Regulates Central Canal Formation and Gait Selection. *Cell Rep* **31**, 107741 (2020).
11. K. Padian, L. M. Chiappe, The origin of birds and their flight. *Sci Am* **278**, 38-47 (1998).
12. K. Straznicky, Function of Heterotopic Spinal Cord Segments Investigation in the Chick. *Acta Biol Acad Sci Hung* **14**, 143-153 (1963).
13. C. H. Narayanan, V. Hamburger, Motility in chick embryos with substitution of lumbosacral by brachial and brachial by lumbosacral spinal cord segments. *J Exp Zool* **178**, 415-431 (1971).
14. N. Rabe Bernhardt *et al.*, DCC mediated axon guidance of spinal interneurons is essential for normal locomotor central pattern generator function. *Developmental biology* **366**, 279-289 (2012).
15. N. Rabe, H. Gezelius, A. Vallstedt, F. Memic, K. Kullander, Netrin-1-dependent spinal interneuron subtypes are required for the formation of left-right alternating locomotor circuitry. *J Neurosci* **29**, 15642-15649 (2009).
16. T. E. Kennedy, T. Serafini, J. R. de la Torre, M. Tessier-Lavigne, Netrins are diffusible chemotropic factors for commissural axons in the embryonic spinal cord. *Cell* **78**, 425-435 (1994).
17. T. Serafini *et al.*, The netrins define a family of axon outgrowth-promoting proteins homologous to C. elegans UNC-6. *Cell* **78**, 409-424 (1994).
18. K. M. Morris *et al.*, The quail genome: insights into social behaviour, seasonal biology and infectious disease response. *BMC Biol* **18**, 14 (2020).
19. P. V. Lovell *et al.*, Conserved syntenic clusters of protein coding genes are missing in birds. *Genome Biol* **15**, 565 (2014).
20. S. Claramunt, J. Cracraft, A new time tree reveals Earth history's imprint on the evolution of modern birds. *Sci Adv* **1**, e1501005 (2015).
21. E. D. Jarvis *et al.*, Whole-genome analyses resolve early branches in the tree of life of modern birds. *Science* **346**, 1320-1331 (2014).
22. R. O. Prum *et al.*, A comprehensive phylogeny of birds (Aves) using targeted next-generation DNA sequencing. *Nature* **526**, 569-573 (2015).

23. A. Rhie *et al.*, Towards complete and error-free genome assemblies of all vertebrate species. *bioRxiv*, 2020.2005.2022.110833 (2020).
24. C. A. Cowan, M. Henkemeyer, The SH2/SH3 adaptor Grb4 transduces B-ephrin reverse signals. *Nature* **413**, 174-179 (2001).
25. Q. Lu, E. E. Sun, R. S. Klein, J. G. Flanagan, Ephrin-B reverse signaling is mediated by a novel PDZ-RGS protein and selectively inhibits G protein-coupled chemoattraction. *Cell* **105**, 69-79 (2001).
26. H. L. Holen *et al.*, Ephrin-B3 binds to a sulfated cell-surface receptor. *Biochem J* **433**, 215-223 (2011).
27. H. L. Holen *et al.*, Ephrin-B3 binds specifically to B lymphocytes in blood and induces migration. *Scand J Immunol* **74**, 144-154 (2011).
28. J. P. Himanen, N. Saha, D. B. Nikolov, Cell-cell signaling via Eph receptors and ephrins. *Curr Opin Cell Biol* **19**, 534-542 (2007).
29. C. N. Arnold *et al.*, ENU-induced phenovariance in mice: inferences from 587 mutations. *BMC Res Notes* **5**, 577 (2012).
30. Y. Jiang *et al.*, The methyltransferase SETDB1 regulates a large neuron-specific topological chromatin domain. *Nat Genet* **49**, 1239-1250 (2017).
31. R. Imondi, Z. Kaprielian, Commissural axon pathfinding on the contralateral side of the floor plate: a role for B-class ephrins in specifying the dorsoventral position of longitudinally projecting commissural axons. *Development* **128**, 4859-4871 (2001).
32. V. Hamburger, R. Oppenheim, Prehatching motility and hatching behavior in the chick. *J Exp Zool* **166**, 171-203 (1967).
33. S. Paixao *et al.*, EphrinB3/EphA4-mediated guidance of ascending and descending spinal tracts. *Neuron* **80**, 1407-1420 (2013).
34. R. Necker, The structure and development of avian lumbosacral specializations of the vertebral canal and the spinal cord with special reference to a possible function as a sense organ of equilibrium. *Anat Embryol (Berl)* **210**, 59-74 (2005).
35. K. Stanchak, C. French, D. Perkel, B. Brunton, The balance hypothesis for the avian lumbosacral organ and an exploration of its morphological variation. *Integrative Organismal Biology* **2**, 1-15 (2020).
36. A. Kusuma, H. J. ten Donkelaar, Propriospinal fibers interconnecting the spinal enlargements in some quadrupedal reptiles. *J Comp Neurol* **193**, 871-891 (1980).
37. R. F. Samara, S. N. Currie, Crossed commissural pathways in the spinal hindlimb enlargement are not necessary for right left hindlimb alternation during turtle swimming. *J Neurophysiol* **98**, 2223-2231 (2007).
38. J. D. Comer *et al.*, Sensory and spinal inhibitory dorsal midline crossing is independent of Robo3. *Front Neural Circuits* **9**, 36 (2015).
39. E. N. Orlino, Jr., C. M. Wong, P. E. Phelps, L1 and GAD65 are expressed on dorsal commissural axons in embryonic rat spinal cord. *Brain Res Dev Brain Res* **125**, 117-130 (2000).
40. G. Kardon, Muscle and tendon morphogenesis in the avian hind limb. *Development* **125**, 4019-4032 (1998).
41. C. Lance-Jones, L. Landmesser, Pathway selection by chick lumbosacral motoneurons during normal development. *Proc R Soc Lond B Biol Sci* **214**, 1-18 (1981).
42. D. Satoh, C. Pudenz, S. Arber, Context-Dependent Gait Choice Elicited by EphA4 Mutation in Lbx1 Spinal Interneurons. *Neuron* **89**, 1046-1058 (2016).
43. I. B. Hogue *et al.*, Fluorescent Protein Approaches in Alpha Herpesvirus Research. *Viruses* **7**, 5933-5961 (2015).
44. Y. Hadas *et al.*, A 'tool box' for deciphering neuronal circuits in the developing chick spinal cord. *Nucleic Acids Res* **42**, e148 (2014).

45. D. H. Rowitch *et al.*, Identification of an evolutionarily conserved 110 base-pair cis-acting regulatory sequence that governs Wnt-1 expression in the murine neural plate. *Development* **125**, 2735-2746 (1998).
46. L. S. Andersson *et al.*, Mutations in DMRT3 affect locomotion in horses and spinal circuit function in mice. *Nature* **488**, 642-646 (2012).
47. V. B. Indjeian *et al.*, Evolving New Skeletal Traits by cis-Regulatory Changes in Bone Morphogenetic Proteins. *Cell* **164**, 45-56 (2016).
48. E. Z. Kvon *et al.*, Progressive Loss of Function in a Limb Enhancer during Snake Evolution. *Cell* **167**, 633-642 e611 (2016).
49. J. P. Himanen *et al.*, Crystal structure of an Eph receptor-ephrin complex. *Nature* **414**, 933-938 (2001).
50. C. E. Restrepo *et al.*, Change in the balance of excitatory and inhibitory midline fiber crossing as an explanation for the hopping phenotype in EphA4 knockout mice. *Eur J Neurosci* **34**, 1102-1112 (2011).
51. R. L. Watterson, Development of the glycogen body of the chick spinal cord; normal morphogenesis, vasculogenesis and anatomical relationships. *J Morphol* **85**, 337-389 (1949).
52. F. Friocourt *et al.*, Recurrent DCC gene losses during bird evolution. *Sci Rep* **7**, 37569 (2017).
53. C. Patthey, Y. G. Tong, C. M. Tait, S. I. Wilson, Evolution of the functionally conserved DCC gene in birds. *Sci Rep* **7**, 42029 (2017).
54. K. D. Phan *et al.*, Neogenin may functionally substitute for Dcc in chicken. *PLoS One* **6**, e22072 (2011).
55. P. Zelina *et al.*, Signaling switch of the axon guidance receptor Robo3 during vertebrate evolution. *Neuron* **84**, 1258-1272 (2014).
56. J. Korlach *et al.*, De novo PacBio long-read and phased avian genome assemblies correct and add to reference genes generated with intermediate and short reads. *Gigascience* **6**, 1-16 (2017).
57. M. Matsunami *et al.*, A comprehensive reference transcriptome resource for the Iberian ribbed newt Pleurodeles waltl, an emerging model for developmental and regeneration biology. *DNA Res* **26**, 217-229 (2019).
58. A. Filosa *et al.*, Neuron-glia communication via EphA4/ephrin-A3 modulates LTP through glial glutamate transport. *Nature neuroscience* **12**, 1285-1292 (2009).
59. Y. Lallemand, V. Luria, R. Haffner-Krausz, P. Lonai, Maternally expressed PGK-Cre transgene as a tool for early and uniform activation of the Cre site-specific recombinase. *Transgenic Research* **7**, 105-112 (1998).
60. M. G. Grabherr *et al.*, Full-length transcriptome assembly from RNA-Seq data without a reference genome. *Nat Biotechnol* **29**, 644-652 (2011).
61. A. Kania, T. M. Jessell, Topographic motor projections in the limb imposed by LIM homeodomain protein regulation of ephrin-A:EphA interactions. *Neuron* **38**, 581-596 (2003).

Acknowledgments

The authors dedicate this paper to the memory of Haya Falk, our dear collaborator and friend, who passed away on November 22. 2019 while this research was in progress. The authors thank Tamir Lederman for technical assistance; Jerome Gros for providing the Pacbio p-reads of the quail genome; Wes Warren for providing the Pacbio p-reads of the chicken genome; Gilgi Friedlander, Moran Yassour and Yotam Drier for assistance in the analysis the expression and regulation data; and Anat Barnea for providing zebra finch hatchlings.

Funding:

This work was supported by a grant to AK and CVM from the US-Israel Binational Science Foundation (grant No. 2017/172), an NSF graduate fellowship to SF, and grants to AK from the Israel Science Foundation (grant No. 1400/16) and the Avraham and Ida Baruch endowment fund.

Author contributions:

AK, CVM, BH: research design, data analysis; BH: circuit analysis, in situ hybridization; OM: circuit analysis; RSM: enhancer analysis; JE: protein studies; SF, PVL: genomics and gene structure analysis; SP, RK: generated conditional EphA4 knockout mouse; AK, CVM: wrote manuscript.

Competing interests:

The authors declare no competing of interest

Data and materials availability:

All data needed to evaluate the conclusions in the paper are present in the paper and/or the Supplementary Materials.

Figures and Tables

Figures legends

Figure 1: Spinal gait circuitry and EFNB3 genomics

A,B. Schematic illustration of the morphology and wiring of the spinal cord in wt mouse (A) and in ephrin-B3/EphA4/α2-chimaerin mice collectively referred to as *hopB3* mutants (B); pre-MN: pre-motoneurons, RP: roof plate. **C.** Simplified cladogram depicting the relations across representative vertebrate groups examined in this study. Branch lengths are arbitrary and not calibrated for time, red means EFNB3 is absent in galliforms, dark blue indicates branches with solid evidence of EFNB3 sequence divergence from non-avian groups, light blue indicates branches with limited EFNB3 sequence data. **D.** Comparison of EFNB3 synteny across representative organisms where synteny could be examined, with chromosomal location or data source indicated. EFNB3 (red) is absent in galliforms (red square) and DNAH2 (blue) is absent in birds. Non-avian sauropsids: lizards (e.g. green anole) and crocodiles (e.g. Chinese alligator); wgs: whole-genome shotgun contigs. **E.** Schematic structure of the predicted mouse and avian ephrin-B3 proteins. RBD: receptor binding domain; TM: transmembrane domain.

Figure. 2: Zebra finch ephrin-B3 protein and mRNA expression

A. The mouse and zebra finch proteins are presented on the cell membrane. An anti-myc antibody (9E10) was used for surface staining of COS-7 cells transiently transfected with amino-terminal myc-tagged ephrin-B3 isoforms. The sequence of the full length zebra finch ephrin-B3 transcript was reconstructed from RNA-seq reads using the Trinity platform (*60*) (Fig. S1). **B.** Binding assay shows EphA4-AP binding to mouse ephrin-B3 protein but not to GFP or to zebra finch ephrin-B3. **C.** Representative EphA4-AP/ephrin-B3 binding curves assessed by AP activity in a colorimetric assay. Apparent KD value for mouse ephrin-B3 was 40.15 nM (n=3).**D.** *In situ* hybridization for ephrin-B3 mRNA in P0 zebra finch spinal cord. High expression is evident in the floor plate (FP), but declines along the roof plate (RP). **D'.** Normalized optical density (OD) profile of zebra finch ephrin-B3 midline expression; shown is the mean from 58 cross sections. **E.** *In situ* hybridization for ephrin-B3 mRNA in E15.5 mouse spinal cord. High expression is evident in both the FP and RP. **E'.** Normalized optical density (OD) profile of mouse ephrin-B3 midline expression; shown is the mean from 160 cross sections. **F,G.** Analysis of the activity of the ephrin-B3 enhancer element, at E9 (F) and E15 (G). The cherry reporter gene was cloned downstream to the putative enhancer and electroporated into the chick spinal cord. GFP, under the control of the ubiquitous CAGG

enhancer-promoter, was co-electroporated. The reporter is detected in both FP and RP (F,G), similar to the pattern of ephrin-B3 expression in mice, while GFP is expressed ubiquitously.

Figure 3: Expression of ephrin-B1, ephrin-B2 and EphA4 mRNAs in the chick spinal cord.
In situ hybridization for ephrin-B1 (A,B), ephrin-B2 (C,D) and EphA4 (E,F) mRNAs at the brachial level in E10 (A,C,E) and E16 (B,D,F) cords. The floor plate (FP) is indicated by black arrows and the roof plate (RP) by magenta arrows. **A,B**. Ephrin-B1 at E10 is high in the FP and low in the RP at E16 it is high in the FP and low in ventral RP. **C,D.** Ephrin-B2 at E10 is low in the FP and RP; at E16 it is low in ventral RP. **E,F.** EphA4 expression at E10 is widespread in the gray matter, with higher levels in scattered interneurons the lateral subdivision of the lateral motor columns (LMC_l) and the medial motor columns (MMC). At E16, expression is detected in scattered interneurons and motoneurons. Interneurons invading the dorsal midline are apparent (white arrow in inset in F). Insets in E and F are enlargements of the areas boxed in dashed yellow. **E',F'.** Cell density distribution, obtained from 10 cross sections from the regions flanking the dorsal midline at E10 and E16, respectively (indicated by white dashed boxes in E and F). **G.** Summation of cell *in situ* hybridization relative intensity in the area indicated in E' (E10, blue) and F' (E16, red values are significantly different at the dorsal midline (t-test, $p<0.05$, n=10 per group).

Figure 4: Spinal cord shows enlarged brachial RPs in *hopB3* mutants, chick and zebra finch.
A-D, Dark field microphotographs of transverse sections of adult mouse spinal cord at lumbar and brachial levels. Compared are control heterozygous ($EphA4^{lx/lx-}$; A,C) and homozygous null mice ($EphA4^{lx/lx-}$/PGK-Cre^{+}; B,D) (*33*). Right insets (enlargements of the boxed areas) depict the central canal and the RP and FP.
E,F. Transverse sections at the brachial (E) and lumbar (F) levels of E15 chick spinal cord. The white matter is labelled with the anti-neurofilament antibody 3A10, the gray matter with nuclear DAPI staining. Right inset (in E) is an enlargement of the boxed area.
G. Transverse section at the brachial level of P8 zebra finch. The white matter is labelled with the anti-neurofilament antibody 3A10. Right inset is an enlargement of the boxed area.
H. Box plot representation of the roof plate (RP) to floor plate (FP) length ratios at the brachial level in adult EphA4+/- mouse (N= 3, 36 cross sections), adult EphA4-/- mouse (N= 3, 36 sections), E15 chick (N= 2, 22 sections) and P0 zebra finch (N= 1, 25 sections). Comparing the RP/FP ratios across groups using Dunnett's method (which takes into account multiple comparisons) shows a

significant differences between the heterozygous mouse and the null mouse, chick and zebra finch. The circle charts shows the significance. No overlapping the heterozygous mouse (red circle) and other groups (black circles) is indicative of p values < than 0.05 (See supplementary statistics). RP: roof plate; FP: floor plate.

Figure 5: Midline crossing at the brachial and lumbar levels of chick spinal cord

A. Dorsal midline crossing at brachial level in E15 chick demonstrated by neurofilament (3A10) immunostaining in transverse sections. Detail views of three examples in insets, left inset is an enlargement of the boxed area in A. Axons cross at the FP (yellow arrows) and the dorsal part of the RP (white arrows). **B.** Dorsal midline crossing at brachial level in E17 chick; the boxed area is enlarged in B' and B''. Anti-3A10 labels all axons, and anti-TAG1/Axonin labels sensory axons. **C.** Dorsal midline crossing is evident following unilateral expression of a reporter gene. GFP under the control of the CAGG enhancer/promoter construct was electroporated at E3 into the left side of the spinal cord. At E15, midline-crossing axons are evident in the brachial FP (yellow arrows) and RP (white arrows) . Detail views of three examples in insets, left inset is an enlargement of the boxed area in C. **D,E.** Transverse sections at the sciatic plexus level at E15 (D) and E17 (E). Axons cross only at the FP (white arrows). The glycogen body (GB) lacks axonal labelling. **F.** Transverse section at the crural plexus level at E17. Right inset is an enlargement of the boxed area in F. Axons cross at the FP (yellow arrow) and RP (white arrow). **G.** Box plot of the ratio between axons crossing the RP and the FP at different axial levels in E15 chick. Numbers of midline-crossing axons were scored at cervical (15 sections), brachial (31 sections), thoracic (27 sections), lumbar crural (23 sections) and lumbar sciatic (14 sections) levels of one embryo. At the sciatic level axons did not cross the glycogen body. (See supplementary statistics). RP: roof plate; FP: floor plate.

Figure 6: Patterns of pre-MNs in the brachial and lumbar chick spinal cord

A-C. Cell distribution maps in the brachial and lumbar segments of E15 spinal cord sections of chicks in which the hindlimb (A), distal wing (B), or pectoral (C) musculature were injected with PRV-cherry at E14. Data are from 1038 ipre-MNs and 88 cpre-MNs in A (3 embryos), 620 ipre-MNs and 210 cpre-MNs in B (4 embryos) and 734 ipre-MNs and 392 cpre-MNs in C (2 embryos). Ellipses in dashed magenta represent the areas occupied by motoneurons. A'-C'. Images of PRV-positive neurons supplemented with immunostaining for motoneurons (ChAT); right insets are

enlargements of the midline boxed area showing axonal decussation of pre-MNs at the FP (yellow arrows) and RP (white arrows); white ellipses represent the central canal.

D. Identification of a subpopulation of pre-MNs that innervate pectoral muscle motoneurons bilaterally. PRV-GFP and PRV-cherry were injected bilaterally at E14 into the pectoral muscles. Cell distribution map of bilaterally innervating pectoral pre-MNs seen at E15 is shown in gray. D'. Examples of bilaterally innervating pre-MNs; left panels: merged images; middle panels: PRV-cherry; right panels: PRV-GFP. Out of 500 and 730 cpre-MNs on each side (18 sections), 11.9% ± 0.05 and 10.9% ± 0.04 were double labeled.

Figure 7: Expression of exogenous ephrin-B3 in the chick RP prevents midline crossing

A. Strategy for ectopic expression of the mouse ephrin-B3 at the roof plate. **B.** Cross-section from brachial spinal cord of E17 embryo expressing ephrin-B3 (magenta) at the dorsal midline, immunostained for neurofilament (cyan). **C,D.** Magnifications of 3 examples of dorsal midline region of spinal cords electroporated with GFP (C,C',C") or ephrin-B3 (D,D',D") (both in magenta), immunostained for neurofilament (cyan). The black and white images are the neurofilament (3A10) staining. Some neurites cross the GFP-expressing RP (C) but not the ephrin-B3-expressing RP. **E.** Quantification of dorsal midline crossing in spinal cords expressing GFP (N=43 sections, 3 embryos), mouse ephrin-B3 (N=71 sections, 3 embryos) or ephrin-B3-ΔC (N=59 sections, 3 embryos). Comparing the number of neurites in the ephrin-B3 and ephrin-b3-ΔC RP to the control (GFP-expressing) RP using Dunnett's method shows a significant difference between the control group and the experimental groups. The circle charts show the significance of these results. No overlapping between the control group (red circle) and the experimental groups (black circles) is indicative of p values < 0.05 (See supplementary statistics). Thus, the numbers of neurites crossing ephrin-B3- or ephrin-B3-ΔC-expressing RPs were significantly lower than in GFP-expressing controls (See supplementary statistics).

Figure 8: Expression of exogenous ephrin-B3 in the chick RP prevents pre-MN crossing

A. Schematic of the experimental setup. GFP or ephrin-B3 were expressed in the midline at E3. At E14, PRV-cherry was unilaterally injected into the wing musculature, and embryos fixed and processed 38 hr later. ChAT-immunostained (cyan) motoneurons (MN)and PRV-labeled (magenta) pre-MNs are indicated; dashed line represents cpre-MN axons that cross the RP. **B,C.** Transverse sections of control (B) and Wnt1::ephrin-B3-expressing E15 embryos (3 examples in C,C'C"). The

black and white images are in B' and the insets in C,C',C" are PRV staining. In the control (B), cpre-MNs somata are located ventral and dorsal to the central canal and neurites of cpre-MNs are apparent at the FP (yellow arrows in B') and RP (white arrows in B'). In Wnt1::mEFNB3 embryos (C, C', C''), the somata of pre-MNs are mainly located ventral to the central canal. Axons crossing the FP (yellow arrows) and few short neurites (white arrowheads) crossing the dorsal midline are shown in the right insets. **D.** Density maps of brachial cpre-MNs in control (GFP, N = 627 cells from three embryos) and five ephrin-B3-expressing embryos (N = 341, 547, 348, 48 and 72 cells). The fraction of sections containing ephrin-B3 expression along the entire dorsal midline is indicated at the upper part of each spinal cord. A ventral shift of the distribution is apparent in the high efficiency electroporated spinal cords of Wnt1-B3-4 and Wnt-1-B3-5.

E. Plot demonstrating the correlation between the percent of dorsal cpre-MNs from all pre-MNs and the electroporation efficiency (as described in D). The average of three GFP-expressing embryos is indicated as a green dot.

Fig. 9: Spinal circuits that enable limb alternation, hopping or flying in mouse and chicken

A,B. Schematic illustration of the morphology and circuit wiring of the spinal cord in wt mouse (A) and in *hopB3* mutants.

C,D. Schematic illustration of the morphology and circuit wiring of the avian spinal cord at the lumbar (C) and brachial (D) leves. We propose that dorsal midline crossing is prevented at the lumbar level by the glycogen body, but enabled at the brachial level due to the loss of ephrin-B3 activity. The brachial avian spinal cord shares significant morphological and wiring similarities with mouse *hopB3* mutants.

E. Schematic illustration of the circuitry at the brachial level of the chick following expression of the mouse ephrin-B3 at the RP. The circuitry resembles that of the wild type mouse (A) and the chick lumbar level (C).

Fig. 1

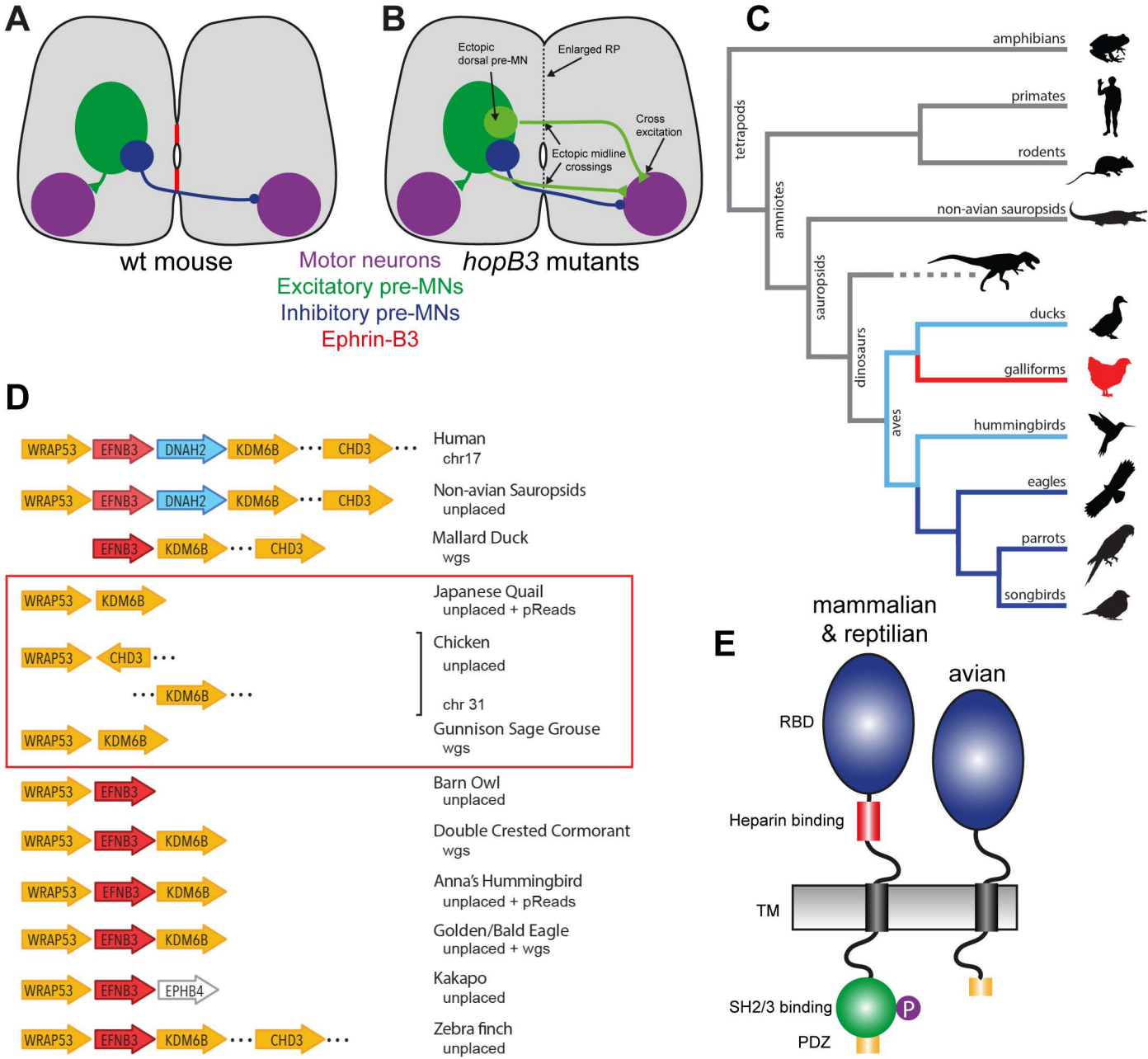
A
B
Ectopic dorsal pre-MN
Enlarged RP
Cross excitation
Ectopic midline crossings
wt mouse
hopB3 mutants
Motor neurons
Excitatory pre-MNs
Inhibitory pre-MNs
Ephrin-B3
C
amphibians
primates
rodents
non-avian sauropsids
ducks
galliforms
hummingbirds
eagles
parrots
songbirds
tetrapods
amniotes
sauropsids
dinosaurs
aves
D
WRAP53
EFNB3
DNAH2
KDM6B
CHD3
EPHB4
Human
chr17
Non-avian Sauropsids
unplaced
Mallard Duck
wgs
Japanese Quail
unplaced + pReads
Chicken
unplaced
chr 31
Gunnison Sage Grouse
wgs
Barn Owl
unplaced
Double Crested Cormorant
wgs
Anna's Hummingbird
unplaced + pReads
Golden/Bald Eagle
unplaced + wgs
Kakapo
unplaced
Zebra finch
unplaced
E
mammalian & reptilian
avian
RBD
Heparin binding
TM
SH2/3 binding
P
PDZ

Figure 2

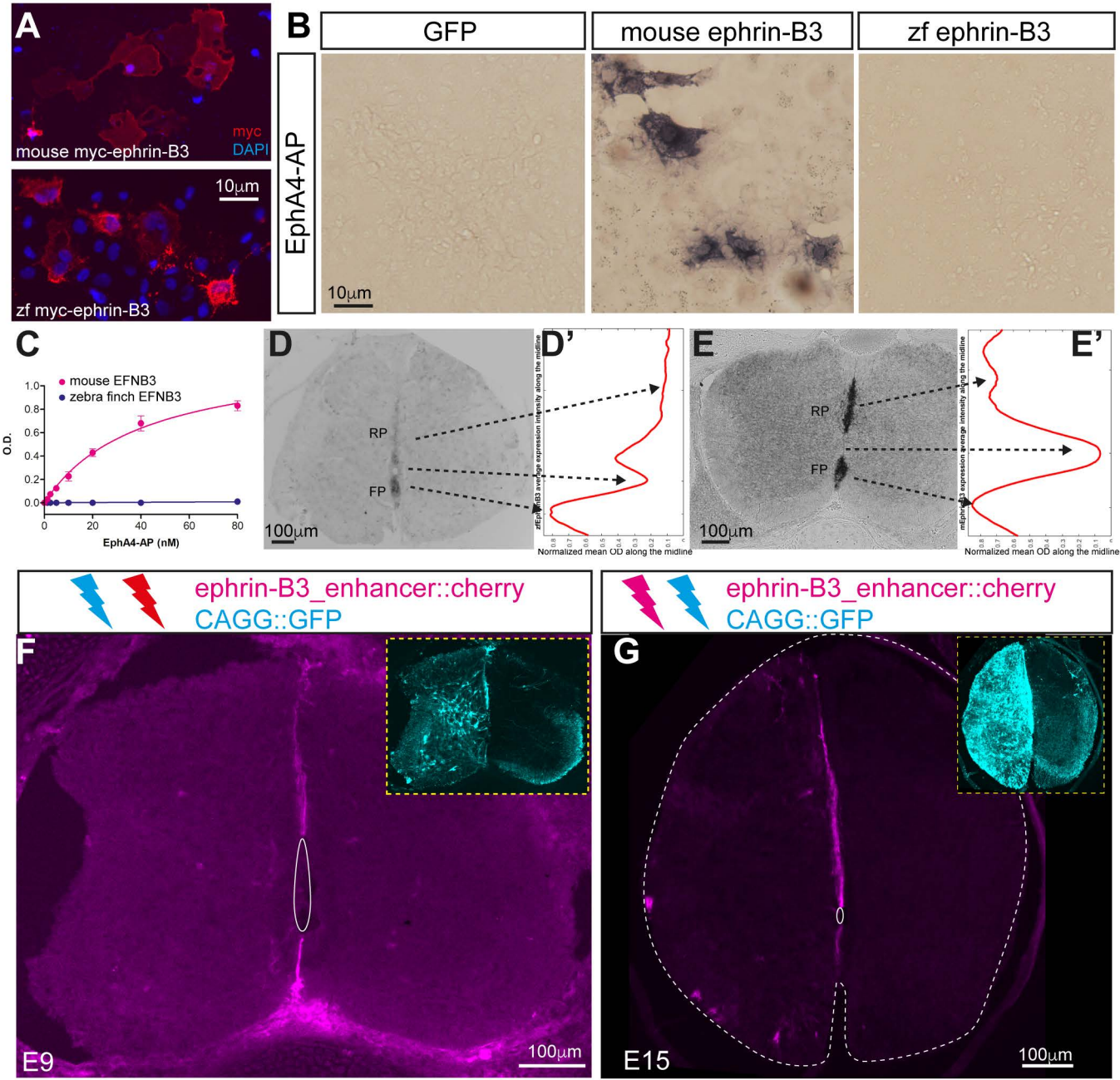
A
mouse myc-ephrin-B3
myc
DAPI
10μm
zf myc-ephrin-B3
B
GFP
mouse ephrin-B3
zf ephrin-B3
EphA4-AP
10μm
C
mouse EFNB3
zebra finch EFNB3
O.D.
EphA4-AP (nM)
D
RP
FP
100μm
D'
Normalized mean OD along the midline
E
RP
FP
100μm
E'
Normalized mean OD along the midline
ephrin-B3_enhancer::cherry
CAGG::GFP
F
E9
100μm
ephrin-B3_enhancer::cherry
CAGG::GFP
G
E15
100μm

Fig. 3

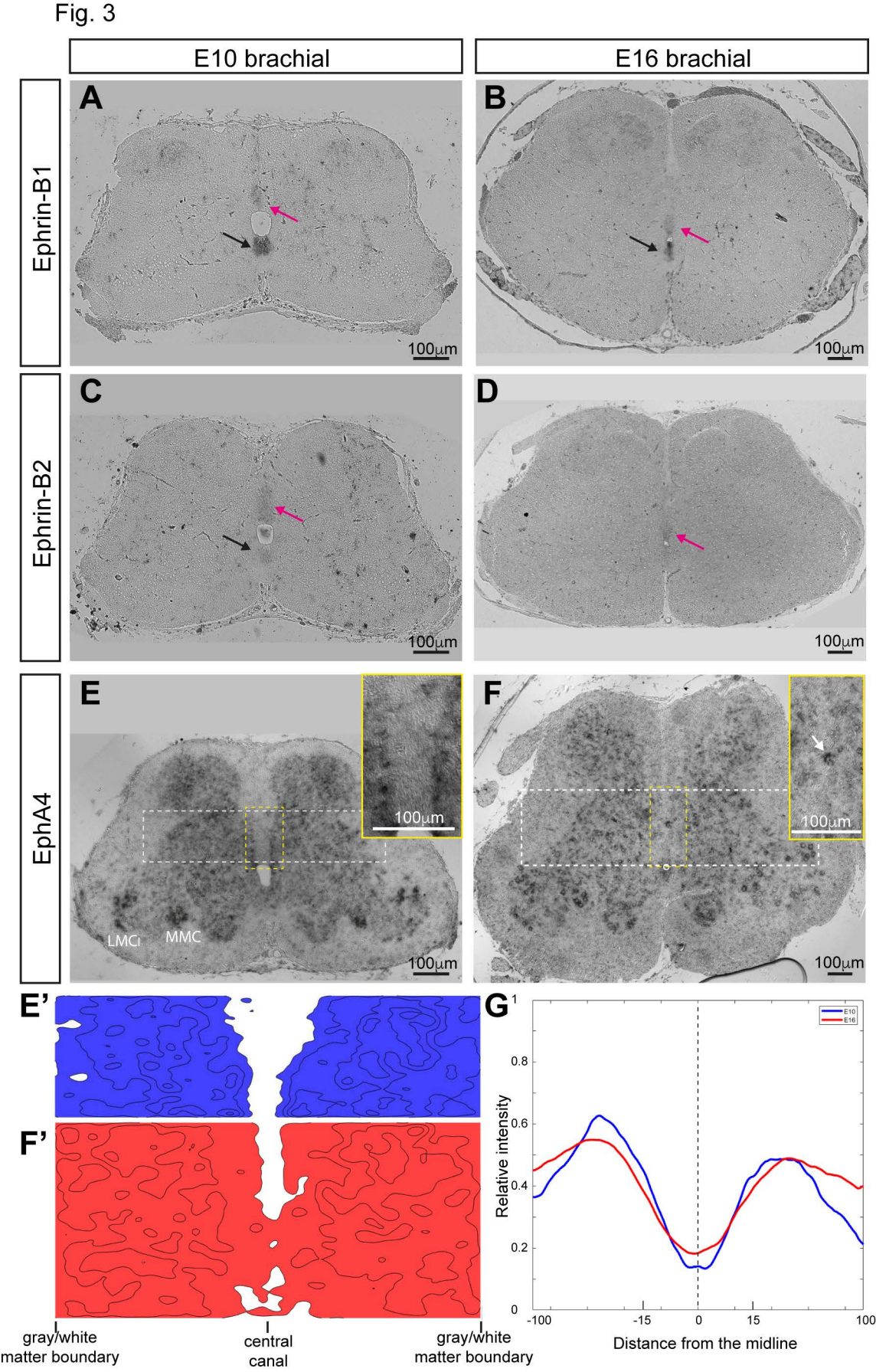
E10 brachial
E16 brachial
Ephrin-B1
Ephrin-B2
EphA4
A
B
C
D
E
F
100μm
LMCl
MMC
E'
F'
G
E10
E16
Relative intensity
Distance from the midline
gray/white matter boundary
central canal
gray/white matter boundary

Fig. 4

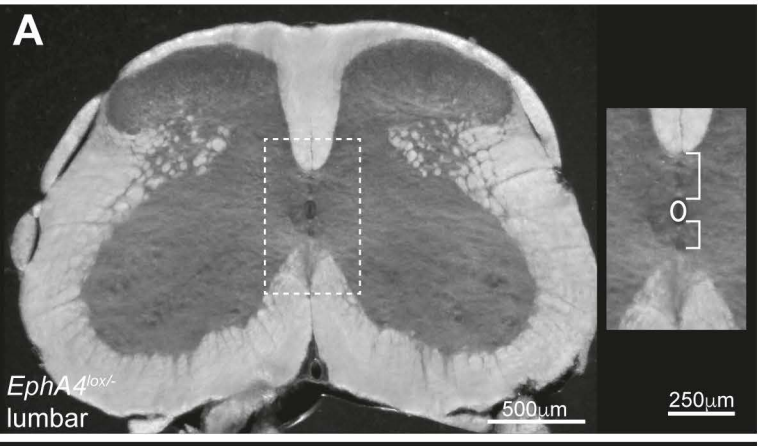
A
EphA4lox/-
lumbar
500µm
250µm

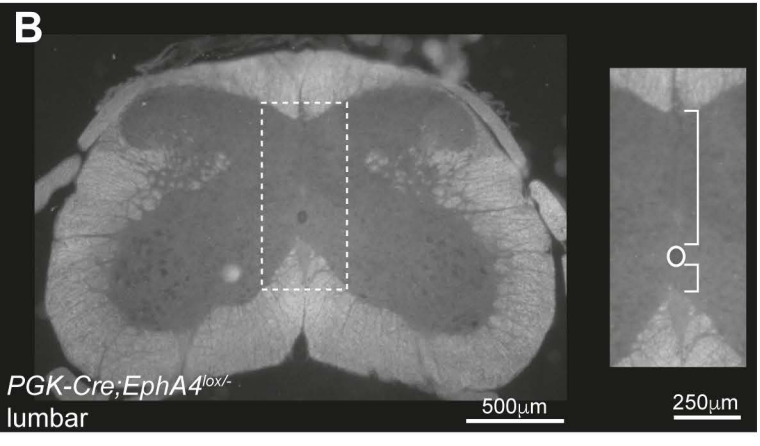
B
PGK-Cre;EphA4lox/-
lumbar
500µm
250µm

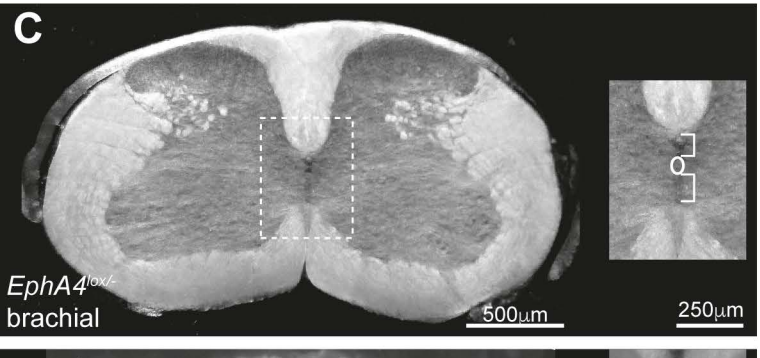
C
EphA4lox/-
brachial
500µm
250µm

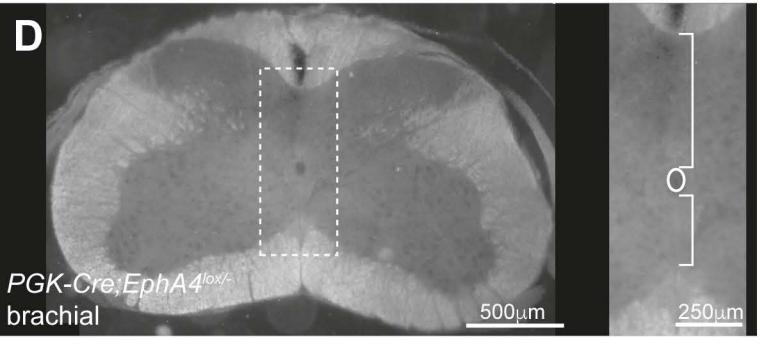
D
PGK-Cre;EphA4lox/-
brachial
500µm
250µm

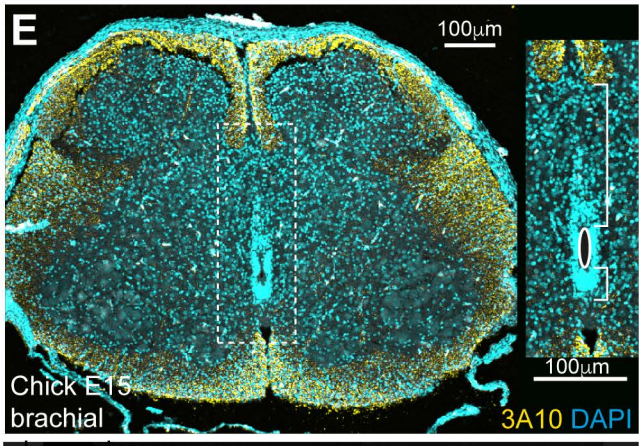
E
100µm
100µm
Chick E15
brachial
3A10 DAPI

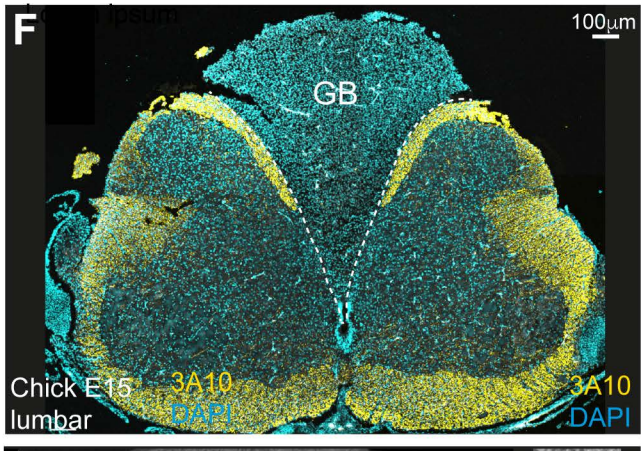
F
100µm
GB
Chick E15
lumbar
3A10
DAPI
3A10
DAPI

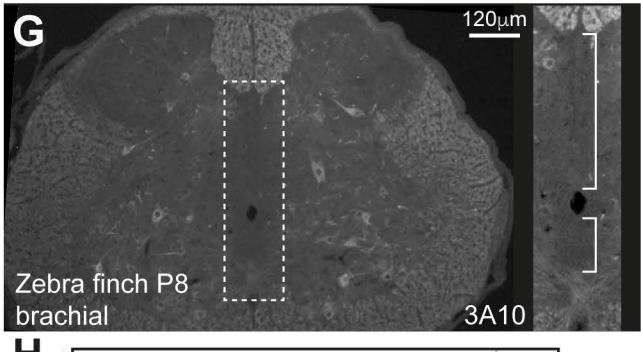
G
120µm
Zebra finch P8
brachial
3A10

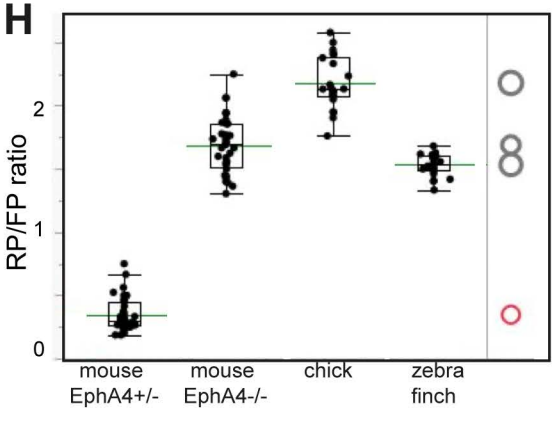
H
RP/FP ratio
0
1
2
mouse
EphA4+/-
mouse
EphA4-/-
chick
zebra
finch

Fig. 5

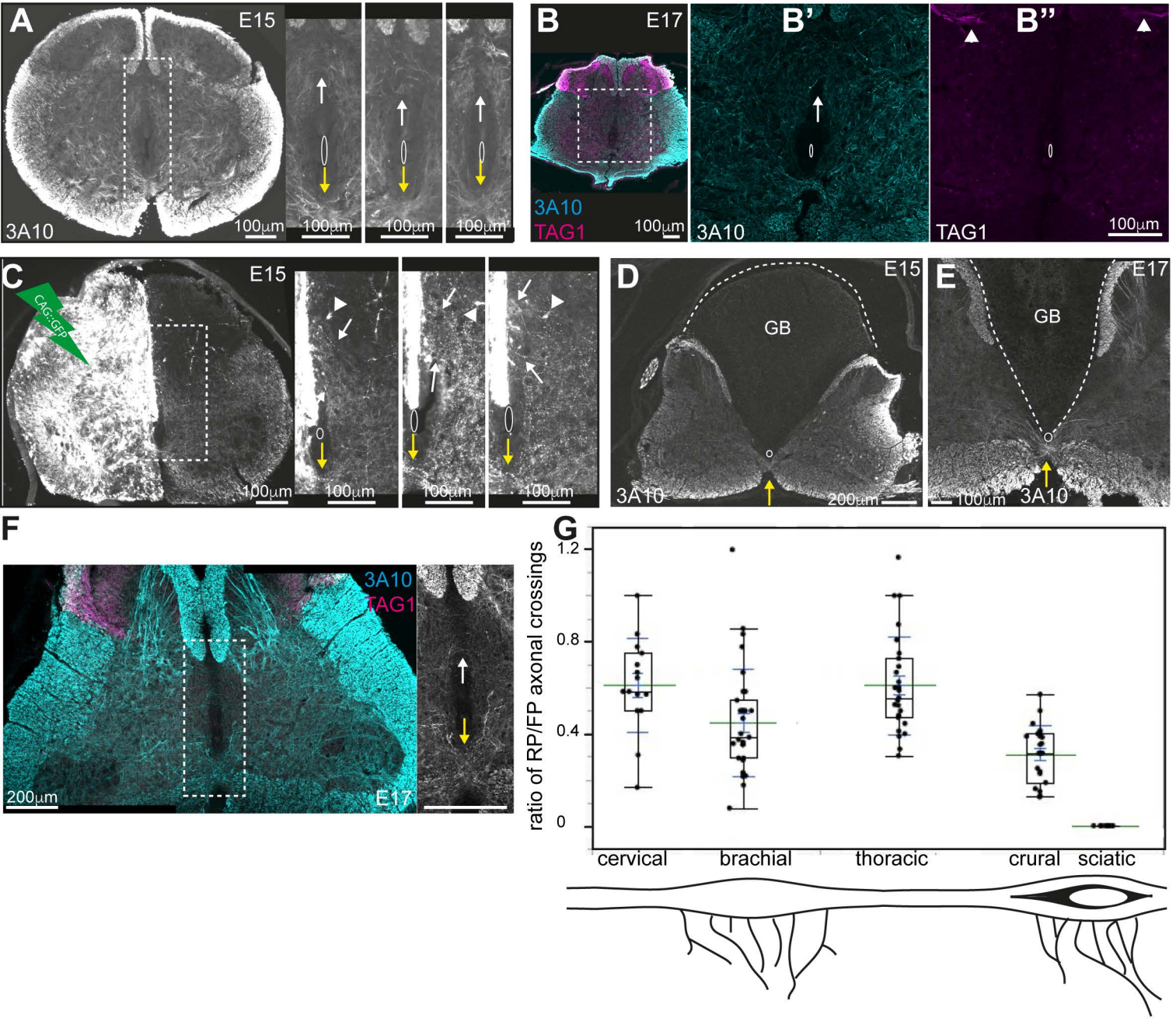
A
E15
3A10
100μm
100μm
100μm
100μm
B
E17
3A10
TAG1
100μm
B'
3A10
B''
TAG1
100μm
C
E15
CAG::GFP
100μm
100μm
100μm
100μm
D
E15
GB
3A10
200μm
E
E17
GB
100μm
3A10
F
3A10
TAG1
200μm
E17
G
ratio of RP/FP axonal crossings
1.2
0.8
0.4
0
cervical
brachial
thoracic
crural
sciatic

Fig. 6

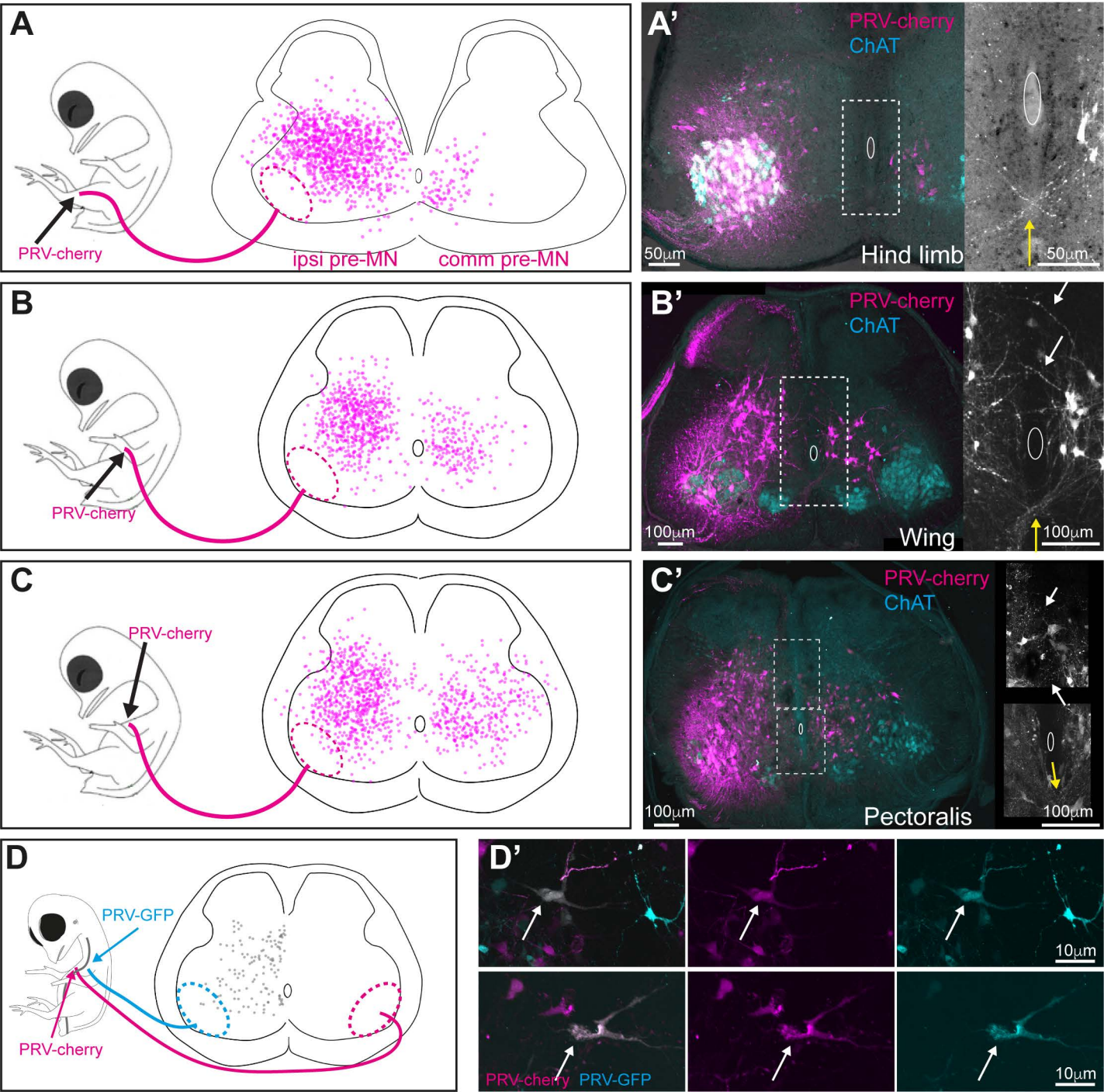
A
PRV-cherry
ipsi pre-MN
comm pre-MN
A'
PRV-cherry
ChAT
50μm
Hind limb
50μm
B
PRV-cherry
B'
PRV-cherry
ChAT
100μm
Wing
100μm
C
PRV-cherry
C'
PRV-cherry
ChAT
100μm
Pectoralis
100μm
D
PRV-GFP
PRV-cherry
D'
10μm
PRV-cherry PRV-GFP
10μm

Fig. 7

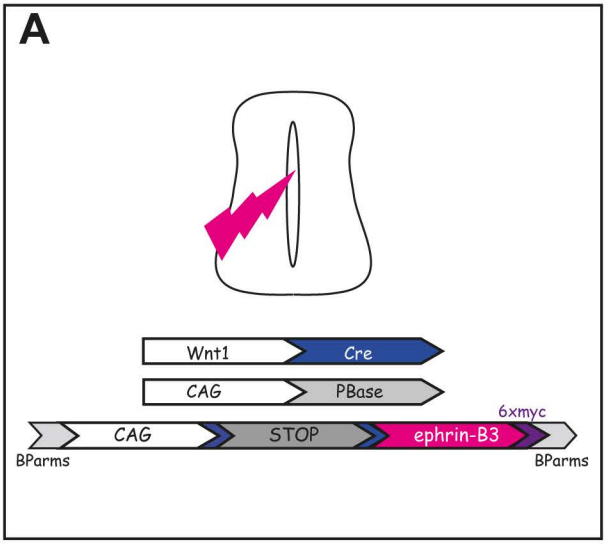
A
Wnt1
Cre
CAG
PBase
6xmyc
CAG
STOP
ephrin-B3
BParms
BParms

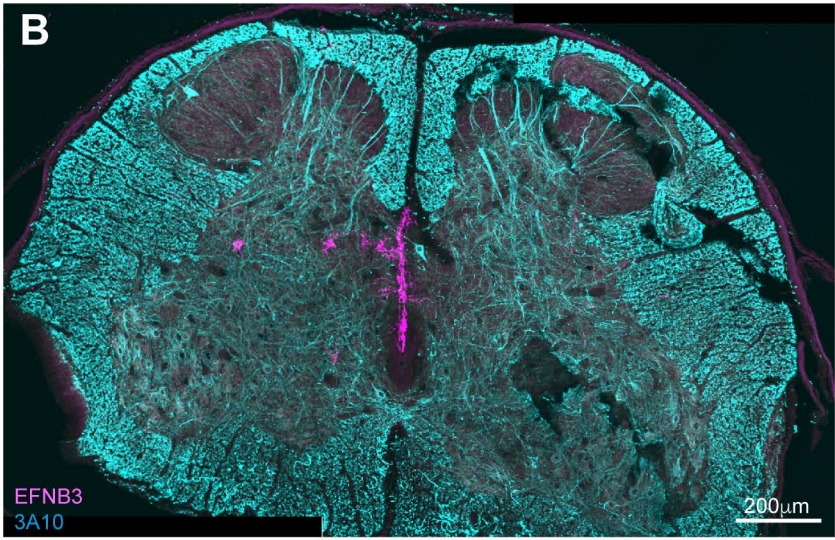
B
EFNB3
3A10
200μm

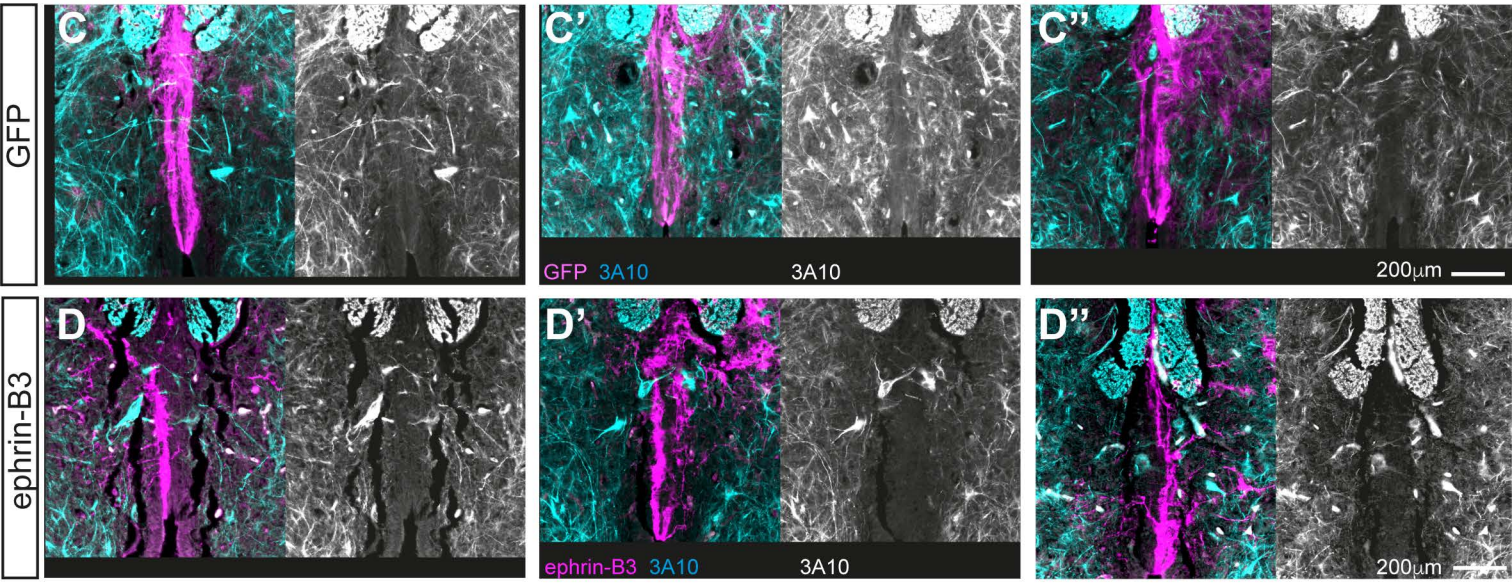
GFP
ephrin-B3
C
C'
C''
D
D'
D''
GFP 3A10
3A10
200μm
ephrin-B3 3A10
3A10
200μm

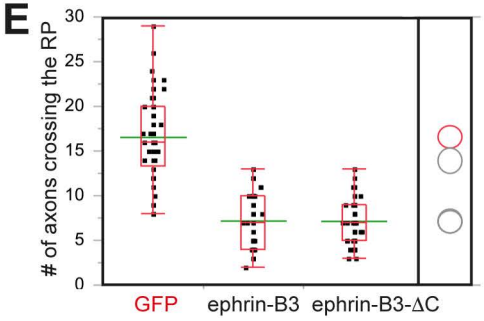
E
# of axons crossing the RP
30
25
20
15
10
5
0
GFP
ephrin-B3
ephrin-B3-ΔC

Fig. 8

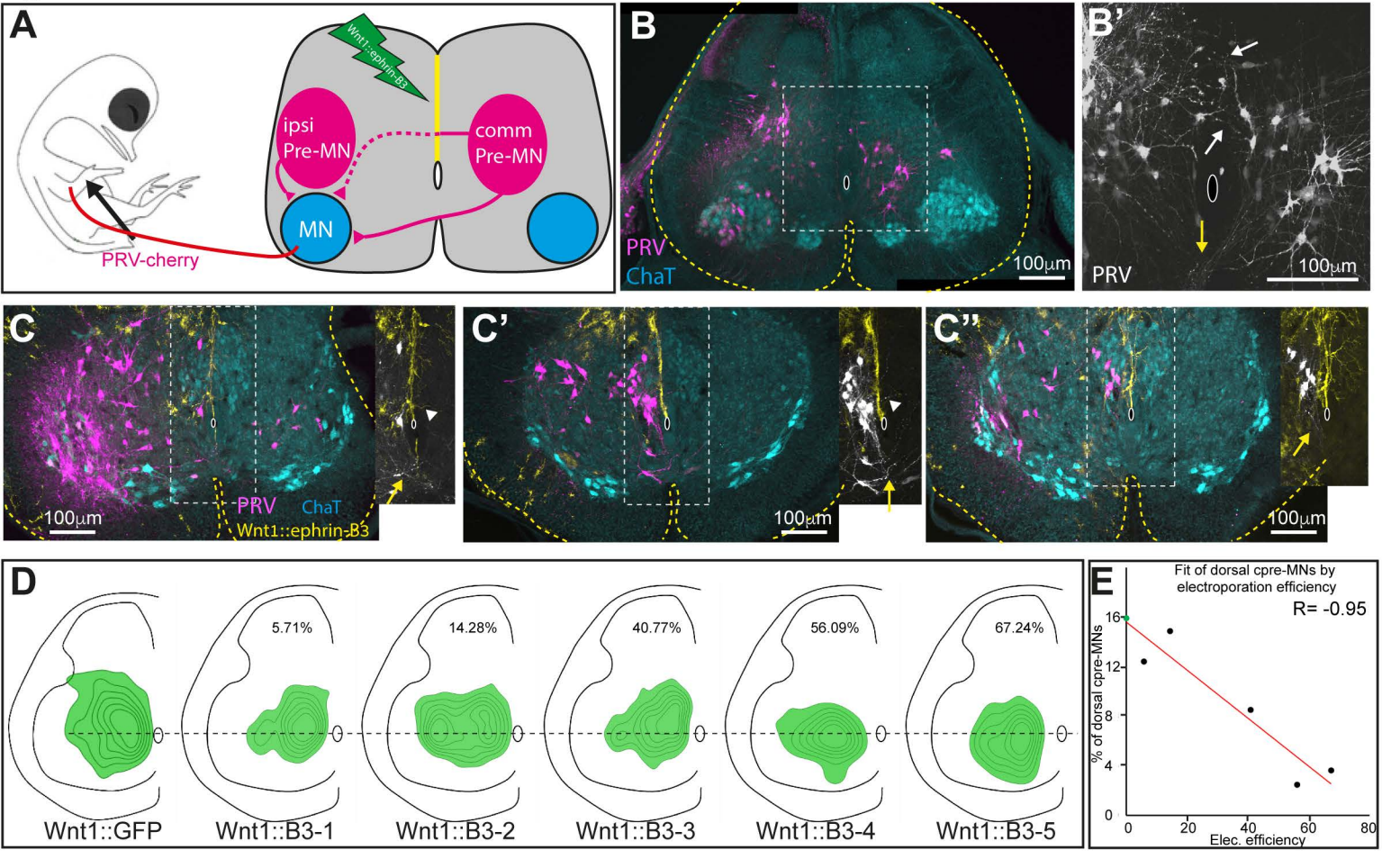
A
Wnt1::ephrin-B3
ipsi
Pre-MN
comm
Pre-MN
MN
PRV-cherry
B
PRV
ChaT
100μm
B'
PRV
100μm
C
100μm
PRV
ChaT
Wnt1::ephrin-B3
C'
100μm
C''
100μm
D
5.71%
14.28%
40.77%
56.09%
67.24%
Wnt1::GFP
Wnt1::B3-1
Wnt1::B3-2
Wnt1::B3-3
Wnt1::B3-4
Wnt1::B3-5
E
Fit of dorsal cpre-MNs by electroporation efficiency
R= -0.95
% of dorsal cpre-MNs
Elec. efficiency
0
4
8
12
16
0
20
40
60
80

Fig. 9

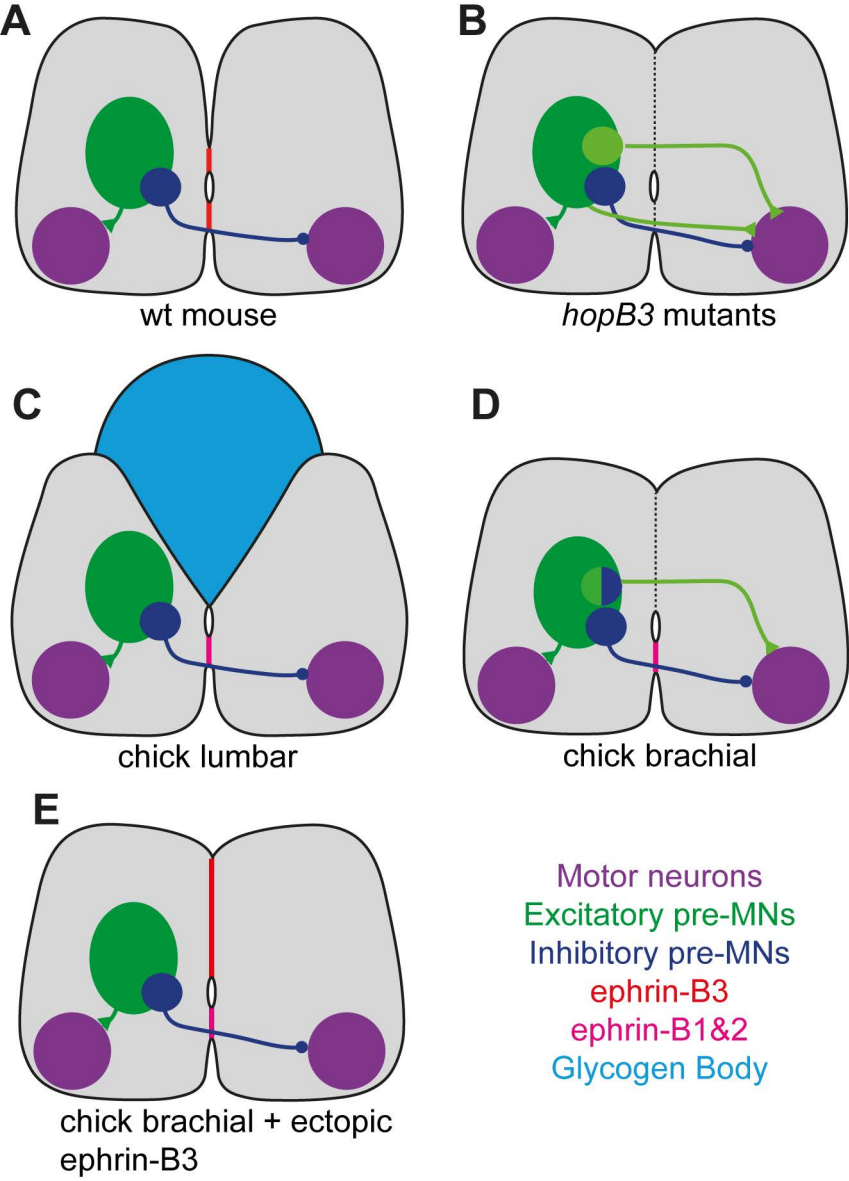
A
wt mouse
B
hopB3 mutants
C
chick lumbar
D
chick brachial
E
chick brachial + ectopic ephrin-B3
Motor neurons
Excitatory pre-MNs
Inhibitory pre-MNs
ephrin-B3
ephrin-B1&2
Glycogen Body

Supplementary Materials for

Natural loss of function of ephrin-B3 shapes spinal flight circuitry in birds

Baruch Haimson[1], Oren Meir[1], Reut Sudakevitz-Merzbach[1], Gerard Elberg[1], Samantha Friedrich[3], Peter V. Lovell[3], Sónia Paixão[2], Rüdiger Klein[2], Claudio V. Mello[3*] and Avihu Klar[1*]

* Avihu Klar. Email: avihu@mail.huji.ac.il
* Claudio V. Mello. Email: melloc@ohsu.edu

This PDF file includes:

Supplementary Text
Figs. S1 to S8
Tables S1-S2
Legend for movie S1
Supplementary statistics

Other Supplementary Materials for this manuscript include the following:
Movies S1

Fig. S1. Ephrin-B3 gene and transcripts in zebra finch

A

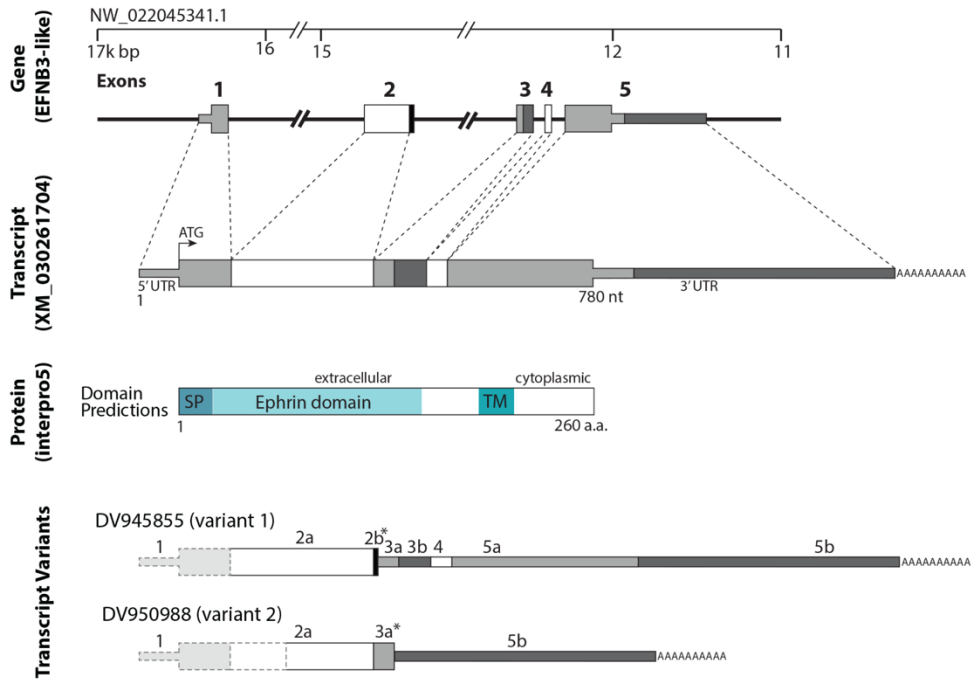

B

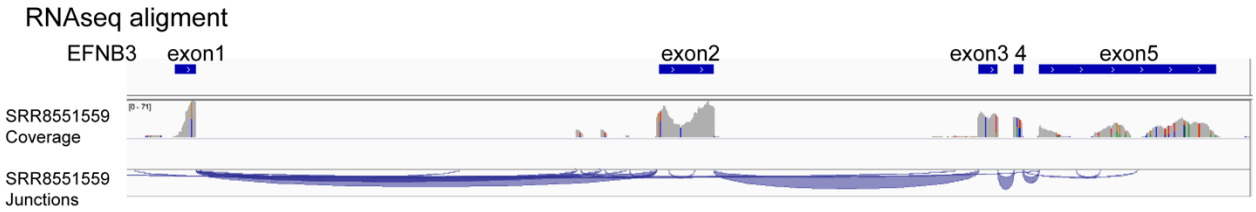

C

```
GGCGGCGGCGGCGGCGGCGGCGGCGGCGGAGCGGGGGGCGGCCGGGGCCCACCGGGAGGGGCCCAGAGCGGC
CGGGGGGCGCCGGGGCCCGGCGGGGCGGGGGGCGATGGCGGGGCGGGCGGCGGCGCTGCTGGTGGCCGTGCTGGG
CGCGGGGGCCGCGGGGCTGAGCCTGGAGCCGGTGGTCTGGCACACGGGGAACCGGCGGTTCCTGGAGGCCGGCGG
TTACGTGCTGTACCCGCAGATCGGTGACCGCCTGGACCTGGTGTGCCCGGGGGGCGCGGGGTACGAGTACTACAA
GCTGTACCTGGTGGGGGGGGCGCAGGCGCGGCGCTGCCAGGTGCCCCCCGCGCCCACCCTGCTGCTGACCTGCGA
CCGCCCCCAGCGCGACGTGCGCTTCACCATCAAGTTCCAGGAGTTCAGCCCCAACCTCTGGGGCCACGAGTTCCG
CCGCCAGCACGACTATTACATCATCACCACCTCGGACGGGACCCCCGAGGGGCTGGAGAACCGCCAGGGCGGGGC
CTGCCTGACCCGGGCCATGCGGGTCACCCTGCGCGTGGGGCAGCGCCCCGGGGCGGAGACACCGCCGGAGCAGGA
TGGGACAGGTTCAGCCAATCAGACGAGCCCGCCCGGGCCGGGCCCGCCCCCCGCGCGGGGAGGGGCGGAGCTGTG
GGGCGCGGGGGGAGGGGCGGCGCTGCTGGCGCTGGGGGGGGCGGGGGGGGCGCTCTGGTGGCGGCGCCGCCCCCG
GAGACCCCCAAAAACTCCACGGGGTGGGGGAGGGGCGGGGCCAACCCGGCCACGCCCCCACGGGCCCGGCCCCGC
CCACCCCCTGCGCGAGCTGCCCCTCCCCCCCGCCGCCCCTCCCCCCACCTACTACAAGGTGTGAGGGGTGGGGGA
GGGGCGGGACACCCAAACTGGGACGGGCCACGCCCACAAAGGGAAGGACACGCCCCACCCTGAAGCTCCGCCCCC
TCGGGGCAAAGGGGAATGACGGACCCAAAAAGGGAAGAATTTGCCCCAAATTGACCCCCCAGGTCTGGATGGGTG
TGGCTTAACCGGGAGGCGTGGCCTGAATTGGGCGTGGTCACTAAAGGGGTGTGGCTGTGATGTCATATGGTGCCG
CCCAGTGGGCGTGGTCAAATATGGGCGTGGTCTCCATAAATGGGCGTGGCTTTACCTGGGGAGGCGGAGCTTAAA
TGGCTTTGAGGCGTCACCCCTGGGAAAGGGGCGGGGCTCGCTCACGGCTCCCTCCCATTGGTCACGATGAAGCCC
CGCCCACACAAAGGGGGCGGAGCTTTCCCGGCGCAGTAACATGGCCGCCGCCACAGCGGATGAACAGGAAGTGAC
GTCACGGCGACAGAGAGGCGGGACTTCCTGTGTGATGTCGCGTGGGGGCGGGGCCTGCGCGCGCGGCTGCTGCTG
ATTAGACAGTTTTGTGCAAAAAAAAAAAAAAAA
```

A. Zebra finch ephrin-B3 gene, predicted transcript, predicted protein, and transcript variants. The two EST clones that include coding exons are DV945855 and DV950988. Both include frameshifts that result in premature termination (indicated by asterisks).
B. RNAseq reads of Ephrin-B3 in zebra finch. RNAseq data in zebra finches provide expression support for this structure and for expression of all five exons, and is consistent with the predicted polyA site based on multiple ESTs.
C. The sequence of the full length zebra finch ephrin-B3 transcript was reconstructed from RNA-seq reads using the Trinity platform. The coding exons are indicated in alternating blue and yellow colors. The 5'UTR (black) is included in the 1st exon and the 3'UTR (black) is included in the 5th exon.
.

Fig. S2. **Phylogeny of the ephrin-B3 protein**

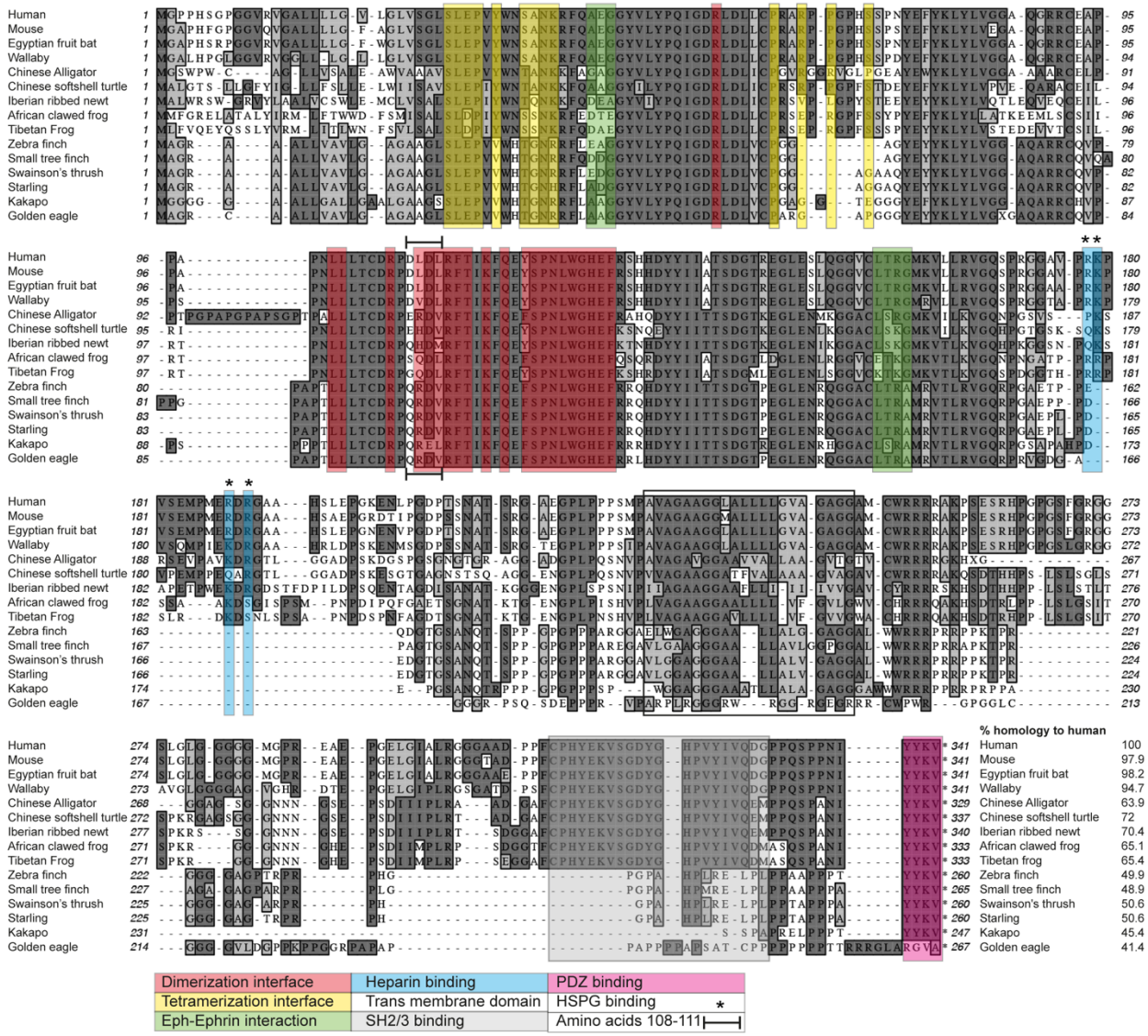

Sequence alignment of the predicted ephrin-B3 proteins from different species representing different modes of locomotion. Human, mouse, alligator and newt use alternating gait; birds and bat fly by synchronous wing flapping; wallaby hops, frogs swim via undulation as the tadpole stage, and by synchronous leg movement in post morphogenesis stage; sea turtles swim by synchronous flapping of their legs, while most sweet water turtle swim by alternate rowing. The T-Coffee algorithm was used for alignment of multiple sequences. The homology to the human protein is indicated at the lower left side. Avian-specific deletions were detected in the heparin binding, tetramerization interface and SH2/3-binding domains (indicated by blue - with asterisks, yellow and gray rectangles, respectively), and specific mutations observed in the dimerization interface domain (indicated by red rectangles and horizontal bars in residues 108-111 of mouse). The open box indicates the transmembrane domain.

Fig. S3: Sequence alignment of EphA4 protein

```
Mouse       1 MAGIFYFILFSFLFGICDAVTGSRVYPANEVTLLDSRSVQGELGWIASPLEGGWEEVSIMDEKNTPIRTYQVCNVMEASQNNWLRTDWITREGAQRVYIE 100
Chick       1 MAGVPVGALLPLLVGVCGAVTGSRVYPANEVTLLDSRSVQGELGWIASPLEGGWEEVSIMDEKNTPIRTYQVCNVMEPSQNNWLRTDWIPREGAQRVYIE 100
Zebra finch 1 MAGVPICALLPLLVGVCGAVTGSRVYPANEVTLLDSRSVQGELGWIASPLEGGWEEVSIMDEKNTPIRTYQVCNVMEPSQNNWLRTDWIPREGAQRVYIE 100

101 IKFTLRDCNSLPGVMGTCKETFNLYYYESDNDKERFIRESQFGKIDTIAADESFTQVDIGDRIMKLNTEIRDVGPLSKKGFYLAFQDVGACIALVSVRVF 200
101 IKFTLRDCNSLPGVMGTCKETFNLYYYESNNDKERFIRESQFAKIDTIAADESFTQVDIGDRIMKLNTEVRDVGPLSKKGFYLAFQDVGACIALVSVRVF 200
101 IKFTLRDCNSLPGVMGTCKETFNLYYYESNNDKERFIRESQFAKIDTIAADESFTQVDIGDRIMKLNTEIRDVGPLSKKGFYLAFQDVGACIALVSVRVF 200

201 YKKCPLTVRNLAQFPDTITGADTSSLVEVRGSCVNNSEEKDVPKMYCGADGEWLVPIGNCLCNAGHEEQNGECQACKIGYYKALSTDASCAKCPPHSYSV 300
201 YKKCPLTVRNLAQFPDTITGADTSSLVEVRGSCVNNSEEKDVPKMYCGADGEWLVPIGNCLCNAGYEERNGECQACKIGYYKALSTDVACAKCPPHSYSI 300
201 YKKCPLTVRNLAQFPDTITGADTSSLVEVRGSCVNNSEEKDVPKMYCGADGEWLVPIGNCLCNAGYEERNGECQACKIGYYKALSTDAACAKCPPHSYSI 300

301 WEGATSCTCDRGFFRADNDAASMPCTRPPSAPLNLISNVNETSVNLEWSSPQNTGGRQDISYNVVCKKCGAGDPSKCRPCGSGVHYTPQQNGLKTTRVSI 400
301 WEGSTSCTCDRGFFRAENDAASMPCTRPPSAPQNLISNVNETSVNLEWSAPQNKGGRDDISYNVVCKRCGAGEPSHCRSCGSGVHFSPQQNGLKTTKVSI 400
301 WEGSTSCTCDRGFFRAESDAASMPCTRPPSAPQHLISNVNETSVNLEWSPPQNKGGREDISYNVVCKRCGAGEPSRCRSCGSGVHFSPQQNGLKSTKVSI 400

401 TDLLAHTNYTFEIWAVNGVSKYNPSPDQSVSVTVTTNQAAPSSIALVQAKEVTRYSVALAWLEPDRPNGVILEYEVKYYEKDQNERSYRIVRTAARNTDI 500
401 TDLLAHTNYTFEVWAVNGVSKHNPSQDQAVSVTVTTNQAAPSPIALIQAKEITRHSVALAWLEPDRPNGVILEYEVKYYEKDQNERSYRIVKTASRNTDI 500
401 TDLLAHTNYTFEVWAVNGVSKQNPSQDQAVSVTVTTNQAAPSPIALIQAKEITRHSVALAWLEPDRPNGVILEYEVKYYEKDQNERSYRIVKTASRNTDI 500

501 KGLNPLTSYVFHVRARTAAGYGDFSEPLFVTTNTVPSRIIGDGANSTVLLVSVSGSVVLVVILIAAFVISRRRSKYSKAKQEADEEKHLNQGVRTYVDPF 600
501 KGLNPLTSYVFHVRARTAAGYGDFSGPFEFTTNTVPSPIIGDGTNPTVLLVSVAGSVVLVVILIAAFVISRRRSKYSKAKQEADEEKHLNQGVRTYVDPF 600
501 KGLNPLTSYVFHVRARTAAGYGDFSGPFEFTTNTVPSPIIGDGTNPTVLLVSVAGSVVLVVILIAAFVISRRRSKYSKAKQEADEEKHLNQGVRTYVDPF 600

601 TYEDPNQAVREFAKEIDASCIKIEKVIGVGEFGEVCSGRLKVPGKREICVAIKTLKAGYTDKQRRDFLSEASIMGQFDHPNIIHLEGVVTKCKPVMIITE 700
601 TYEDPNQAVREFAKEIDASCIKIEKVIGVGEFGEVCSGRLKVPGKREICVAIKTLKAGYTDKQRRDFLSEASIMGQFDHPNIIHLEGVVTKCKPVMIITE 700
601 TYEDPNQAVREFAKEIDASCIKIEKVIGVGEFGEVCSGRLKVPGKREICVAIKTLKAGYTDKQRRDFLSEASIMGQFDHPNIIHLEGVVTKCKPVMIITE 700

701 YMENGSLDAFLRKNDGRFTVIQLVGMLRGIGSGMKYLSDMSYVHRDLAARNILVNSNLVCKVSDFGMSRVLEDDPEAAYTTRGGKIPIRWTAPEAIAYRK 800
701 YMENGSLDAFLRKNDGRFTVIQLVGMLRGIGSGMKYLSDMSYVHRDLAARNILVNSNLVCKVSDFGMSRVLEDDPEAAYTTRGGKIPIRWTAPEAIAYRK 800
701 YMENGSLDAFLRKNDGRFTVIQLVGMLRGIGSGMKYLSDMSYVHRDLAARNILVNSNLVCKVSDFGMSRVLEDDPEAAYTTRGGKIPIRWTAPEAIAYRK 800

801 FTSASDVWSYGIVMWEVMSYGERPYWDMSNQDVIKAIEEGYRLPPPMDCPIALHQLMLDCWQKERSDRPKFGQIVNMLDKLIRNPNSLKRTGSESSRPNT 900
801 FTSASDVWSYGIVMWEVMSYGERPYWDMSNQDVIKAIEEGYRLPPPMDCPIALHQLMLDCWQKERSDRPKFGQIVNMLDKLIRNPNSLKRTGSESSRPST 900
801 FTSASDVWSYGIVMWEVMSYGERPYWDMSNQDVIKAIEEGYRLPPPMDCPIALHQLMLDCWQKERSDRPKFGQIVNMLDKLIRNPNSLKRTGSESSRPST 900

901 ALLDPSSPEFSAVVSVGDWLQAIKMDRYKDNFTAAGYTTLEAVVHMSQDDLARIGITAITHQNKILSSVQAMRTQMQQMHGRMVPV*  987
901 ALLDPSSPEFSAVVSVSDWLQAIKMERYKDNFTAAGYTTLEAVVHMNQDDLARIGITAITHQNKILSSVQAMRSQMQQMHGRMVPV*  987
901 ALLDPSSPEFSAVVSVSDWLQAMKMERYKDNFTAAGYTTLEAVVHMNQEDLARIGITALAHQNKILSSVQAMRTQMQQMHGRMVPV*  987
```

Sequence alignment of EphA4 proteins from mouse, chick and zebra finch. The T-Coffee algorithm was used for alignment of multiple sequences.

Fig. S4. **A putative EFNB3 enhancer in mouse DNAH2**

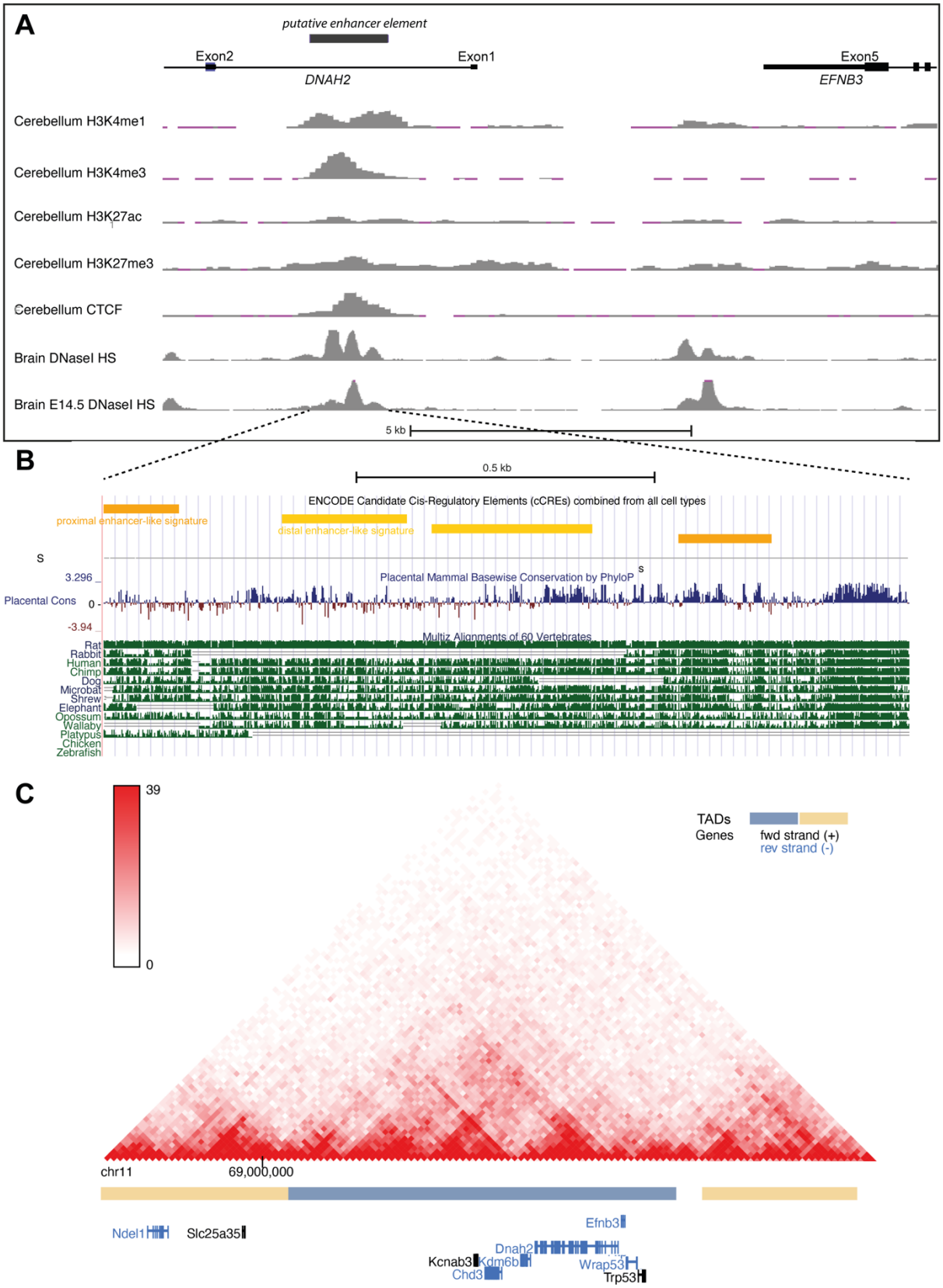

A. A display of ENCODE analysis (mm9 assembly; https://genome.ucsc.edu/index.html) chr11:69,546,195-69,547,544; shown is the region that includes EFNB3 (exons 3-5) and DNAH2 (exons 1-2) genes on the minus strand. A DNAaseI hypersensitive (HS) site is in the 1st intron of DNAH2 (chr11:69,546,195-69,547,544 in GRCm38/mm10). This motif binds modified histones (H3K4me3, H3K4me1 and H3K27ac) that are associated with active enhancers; histone H3K27me3 is associated with repression of developmental genes, as well as CTCF – a nuclear factor associated with active enhancers. Binding of these proteins is apparent in the mouse embryonic cerebellum and brain. The data was obtained from UCSC genome browser.
B. A display of ENCODE analysis (mm10; assembly; https://genome.ucsc.edu/index.html) of the putative ephrin-B3 enhancer. Sequence conservation with various vertebrates is indicated.
C. Hi-C analysis, resolution of 10Kb, of the genomic region that includes EFNB3 and its flanking genes, in cortical neurons (*2*). DNAH2, that includes the putative enhancer, and EFNB3, reside on the same TAD (the grey rectangle).

Fig. S5. **RP/FP ratio along the longitudinal axis of wt mice**

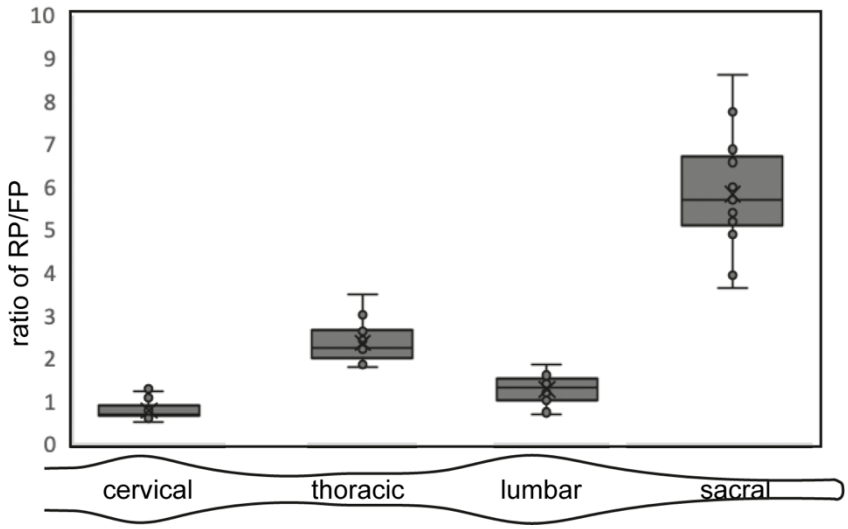

The ratio between the roof plate and floor plate lengths at different segmental levels. The limb-innervating segments exhibit a lower RP/FP ratio compared to the thoracic and sacral levels. Analysis was done on images from the Mouse spinal cord atlas (Allen Institute for Brain Science; N = 17 mice, 15-16 section per mouse). Box plot representation of the roof plate (RP) to floor plate (FP) length ratios at the cervical, thoracic, lumbar and sacral levels at P4.

Fig. S6. **Distribution of pre-MNs at the spinal crural plexus level**

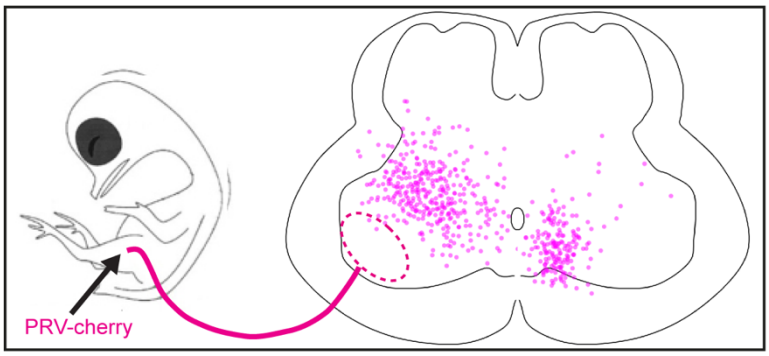

pre-MN map at the crural lumbar level; shown are 361 ipre-MNs and 192 cpre-MNs, respectively (N=3 embryos).

Fig. S7. **Brachial pre-MN neurotransmitter identity**

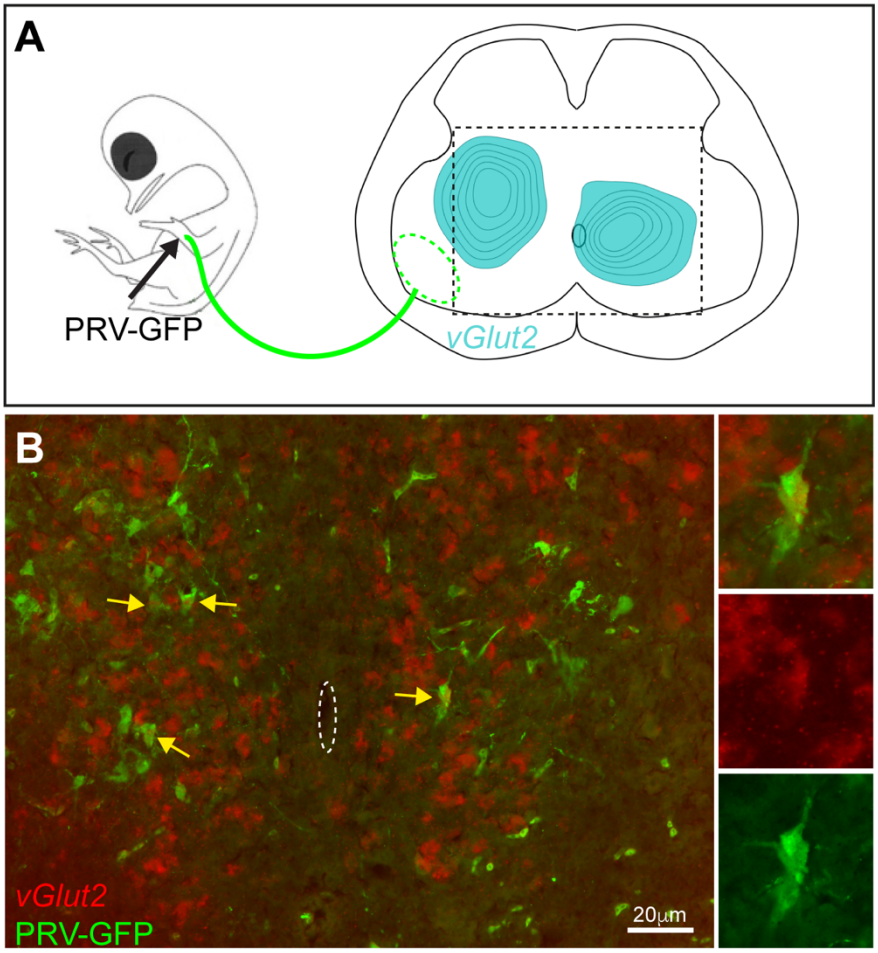

A. Experimental design for brachial pre-MN labeling and *in situ* hybridization for VGlut2. Density maps of ipre-MNs and cpre-MNs are shown. The doted rectangle indicates the position of the image in B.

B. Image of the combined in situ hybridization for *vGlute2* and GFP immunohistochemistry. The yellow arrows point to double stained pre-MNs. The insets on the right side are enlargements and the red and green channels of the commissural pre-MN (at the right side of the spinal cord).

Fig. S8: **Expression of exogenous ephrin-B3 in the chick RP is negatively correlated to the amount of dorsal commissural pre-MNs**

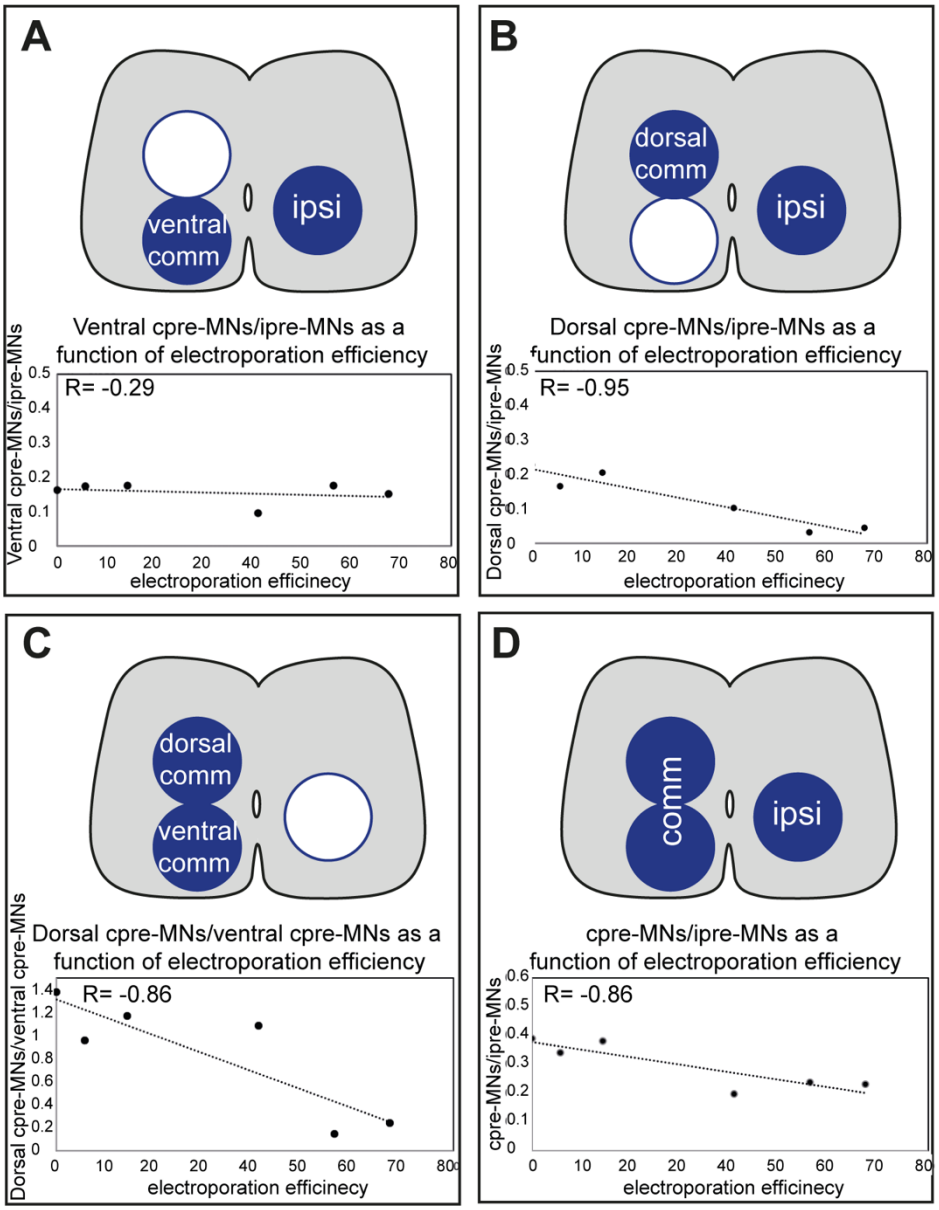

A-D. Plots demonstrating the correlation between ventral commissural/ipsilateral, dorsal commissural/ipsilateral,dorsal commissural/ ventral commissural and commissural/Ipsilateral pre-MNs ratios to the electroporation efficiency (as described in Fig. 8D).

Table S1. The ratio of excitatory pre-MNs in the lumbar and brachial levels of the chick spinal cord.

level	side	% vGlut2	#
Lumbar sciatic	ipsi	46.46	145
	comm	38.62	145
brachial	ipsi	35	274
	Ventral comm	38	29
	Dorsal comm	47	51

Table S2: The number of pre-MNs in the spinal cord following ephrin-B3 ectopic expression

	GFP1	**GFP2**	**GFP3**	Eph1	Eph2	Eph3	Eph4	Eph5	Fig.
Ipsi pre-MN	1002	465	215	1004	1435	1774	193	312	
Comm pre-MN	334	239	54	341	547	348	48	72	
Ventral cpre-MN	148	90	20	174	252	167	42	58	
Dorsal cpre-MN	186	149	34	167	295	181	6	14	
%dcomm/pMN	13.92216	21.16477	12.63941	12.41636	14.88396	8.529689	2.489627	3.645833	8E
vcomm/ipsi	0.147705	0.193548	0.093023	0.173307	0.17561	0.094138	0.217617	0.185897	S8A
dcomm/ipsi	0.185629	0.32043	0.15814	0.166335	0.205575	0.102029	0.031088	0.044872	S8B
dcomm/vcomm	1.256757	1.655556	1.7	0.95977	1.170635	1.083832	0.142857	0.241379	S8C
comm/ipsi	0.333333	0.513978	0.251163	0.339641	0.381185	0.196167	0.248705	0.230769	S8D

PRV labelled neuron were scored in the ipsi lateral spinal cord (ipsi preMN), the contralateral side of the spinal cord (Comm pre-MN), the ventral and dorsal contralateral side of the spinal cord (Ventral cpre-MN and dorsal cpre-MN, respectively). The ratio between the different zones are indicated in the lower five rows. Reference to the relevant plot is indicated in the last column.

Supplementary Movie S1: Confocal z-stack movie of commissural pre-MN crossing the roof plate of an ephrin-B3-expressing embryo.

Confocal image stacks of the roof plate (z-plain - 60μm) of E15.5 chick spinal cord. The roof plate cells express an exogenous ephrin-B3 (green) and pre-MN neurons are labelled by wing-infected PRV-cherry (red). Z-stack images are shown on the left, and indicated by a white cursor on the x-axis image (right side). Neurites of a commissural pre-MN cross the RP through non-ephrin-B3 expressing cells.

Supplementary Statistical Analysis

Fig. 4H.

Quantiles

Level	Minimum	10%	25%	Median	75%	90%	Maximum
1_Mouse EphA4 Het (n=3)	0.1875	0.2	0.266667	0.296703	0.450321	0.535417	0.75
2_Mouse EphA4 KO(n=3)	1.304348	1.396667	1.508333	1.699095	1.857143	1.979861	2.25
3_Chicken (n=2)	1.76087	1.917544	2.06875	2.132456	2.385346	2.482353	2.578947
4_ZF (n=1)	1.333333	1.405848	1.491071	1.536585	1.604167	1.622017	1.681818

Means and Std Deviations

Level	Number	Mean	Std Dev	Std Err Mean	Lower 95%	Upper 95%
1_Mouse EphA4 Het (n=3)	36	0.3476214	0.1355198	0.0225866	0.3017681	0.3934747
2_Mouse EphA4 KO(n=3)	36	1.6895941	0.2226598	0.03711	1.6142568	1.7649313
3_Chicken (n=2)	22	2.1805534	0.2087605	0.0445079	2.0879941	2.2731126
4_ZF (n=1)	25	1.5334836	0.0831688	0.0166338	1.4991531	1.567814

Means Comparisons

Comparisons with a control using Dunnett's Method

Control Group = 1_Mouse EphA4 Het (n=3)

Confidence Quantile

|d|	Alpha
2.39255	0.05

LSD Threshold Matrix

Level	Abs(Dif)-LSD	p-Value
3_Chicken (n=2)	1.721	<.0001*
2_Mouse EphA4 KO(n=3)	1.244	<.0001*
4_ZF (n=1)	1.078	<.0001*
1_Mouse EphA4 Het (n=3)	-0.1	1.0000

Positive values show pairs of means that are significantly different.

Fig. 5G

Quantiles

Level	Minimum	10%	25%	Median	75%	90%	Maximum
Cervical	0.166667	0.251282	0.5	0.583333	0.75	0.9	1
Brachial	0.076923	0.214907	0.294118	0.384615	0.545455	0.822222	1.2
Thorax	0.304348	0.377778	0.470588	0.555556	0.727273	1	1.166667
Crural	0.125	0.131594	0.1875	0.315789	0.4	0.477778	0.571429
Sciatic	0	0	0	0	0	0	0

Means and Std Deviations

Level	Number	Mean	Std Dev	Std Err Mean	Lower 95%	Upper 95%
Cervical	15	0.6103012	0.2033028	0.0524926	0.4977158	0.7228865
Brachial	31	0.4487473	0.2349142	0.0421918	0.36258	0.5349145
Thorax	27	0.6096124	0.2135042	0.0410889	0.525153	0.6940719
Crural	23	0.311106	0.1260886	0.0262913	0.2565812	0.3656308
Sciatic	14	0	0	0	0	0

Fig. 7E.

Quantiles

Level	Minimum	10%	25%	Median	75%	90%	Maximum
GFP	8	9.9	13.25	16	20	23	29
mEFNB3	2	4	4	7	10	12	13
mEFNB3-S	3	4	5	7	9	11	13
zf-EFNB3	9	9	11	13	16	21	21

Means and Std Deviations

Level	Number	Mean	Std Dev	Std Err Mean	Lower 95%	Upper 95%
GFP	48	16.5208	4.72202	0.68156	15.150	17.892
mEFNB3	42	7.1667	3.21518	0.49611	6.165	8.169
mEFNB3-S	47	7.1277	2.66717	0.38905	6.345	7.911
zf-EFNB3	39	13.9744	3.72394	0.59631	12.767	15.182

Means Comparisons

Comparisons with a control using Dunnett's Method

Control Group =
GFP

LSD Threshold Matrix

Level	Abs(Dif)-LSD	p-Value
GFP	-1.78	1.0000
zf-EFNB3	0.663	0.0045*
mEFNB3	7.509	<.0001*
mEFNB3-S	7.601	<.0001*

Positive values show pairs of means that are significantly different.

Fig. 8E

Linear Fit

Dorsal cpre-MNs (dCOMM) = 15.595123 - 0.1938984* elec efficiency

Summary of Fit

RSquare	0.904912
RSquare Adj	0.881141
Root Mean Square Error	1.967219
Mean of Response	9.645707
Observations (or Sum Wgts)	6

Analysis of Variance

Source	DF	Sum of Squares	Mean Square	F Ratio
Model	1	147.31547	147.315	38.0665
Error	4	15.47980	3.870	Prob > F
C. Total	5	162.79527		0.0035*

Parameter Estimates

Term	Estimate	Std Error	t Ratio	Prob>|t|
Intercept	15.595123	1.254921	12.43	0.0002*
elec efficiency	-0.193898	0.031427	-6.17	0.0035*

Multivariate Correlations

	dorsal elec efficiency	dCOMM
elec efficiency	1.0000	-0.9513
dCOMM	-0.9513	1.0000

The correlations are estimated by Row-wise method.

Scatterplot Matrix

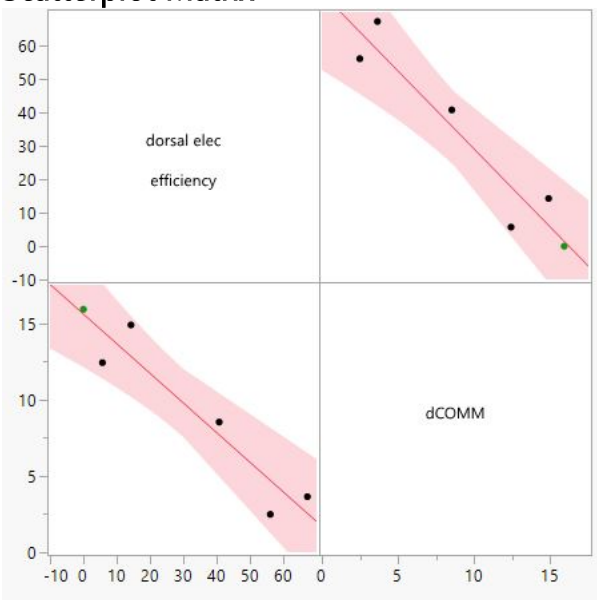

Pairwise Correlations

Variable	by Variable	Correlation	Count	Lower 95%	Upper 95%	Signif Prob
dCOMM	elec efficiency	-0.9513	6	-0.9948	-0.6128	0.0035*